TA 8.

FORSCHUNG - AUSBILDUNG - WEITERBILDUNG

Bericht Nr. 60

A 2-D KANIEL KINETICAL SCHEME FOR THE ISENTROPIC COMPRESSIBLE FLOW

Manfred Bäcker, Helmut Neunzert,
Subbiah Sundar, Suhail Younis

UNIVERSITÄT KAISERSLAUTERN
Fachbereich Mathematik
Arbeitsgruppe Technomathematik
Postfach 3049
6750 Kaiserslautern

September 1991

A 2-D KANIEL KINETICAL SCHEME FOR THE ISENTROPIC COMPRESSIBLE FLOW

S. Sundar, S. Younis, M. Baecker and H. Neunzert
Department of Mathematics
University of Kaiserslautern
P.O. Box 3049
D-6750 Kaiserslautern, Germany

ABSTRACT

We have presented here a two-dimensional kinetical scheme for equations governing the motion of a compressible flow of an ideal gas (Air) based on the Kaniel method. The basic flux functions are computed analytically and have been used in the organization of the flux computation. The algorithm is implemented and tested for the 1D shock and 2D shock-obstacle interaction problems.

1. INTRODUCTION

The equations governing the motion of a smooth inviscid compressible flow are:

$$\frac{\partial \rho}{\partial t} + \sum_i \frac{\partial}{\partial x_i}(\rho u_i) = 0 \tag{1.1}$$

$$\frac{\partial u_i}{\partial t} + \sum_j u_j \frac{\partial u_i}{\partial x_j} + \frac{1}{\rho}\frac{\partial p}{\partial x_i} = 0 \tag{1.2}$$

$$\frac{\partial S}{\partial t} + \sum_i u_i \frac{\partial S}{\partial x_i} = 0 \tag{1.3}$$

$$p = F(\rho, S) \tag{1.4}$$

The scalar $\rho(x,t)$ denotes the density; the vector $u(x,t)$ denotes the velocity; $p(x,t)$ is the pressure; $S(x,t)$ is the entropy and F is a general equation of state. The equations are formulated for points (x,t) where x is an n-dimensional vector (in our case $n=2$).

Equations (1.1) and (1.2) can be written as

$$\frac{\partial \rho}{\partial t} + \sum_i \frac{\partial}{\partial x_i}(m_i) = 0 \tag{1.5}$$

$$\frac{\partial m_i}{\partial t} + \sum_j \frac{\partial}{\partial x_j}\left(\frac{m_i m_j}{\rho}\right) + \frac{\partial p}{\partial x_i} = 0 \tag{1.6}$$

where $m(x,t)$ is the momentum vector with $m(x,t)=\rho u(x,t)$. Equation (1.3) is usually replaced by the equation of conservation of energy, but the equation of state (1.4) is general.

This paper deals with isentropic flow, i.e. entropy is taken to be constant. It is an important special case as there are variety of problems where the assumption of constant entropy causes a negligible error. So, we are mainly considering the equations (1.5) and (1.6) with $p=F(\rho)$.

In recent years there exists a variety of kinetical and Boltzmann schemes dealing with the numerical solution of Euler equations, especially, the flux vector splitting method of Deshpande[1] and the Boltzmann scheme of Perthame[2] are to be noted here. The method dealt here was constructed by Kaniel[3-5] and is based on a kinetic model built for the fluid motion, which was originated by Maxwell[6]. In this model a distribution function $f(x,\xi,t)$ is considered as such that it is the distribution of molecules located at x and having velocity ξ. The density $\rho(x,t)$ and the momentum $m(x,t)$ are then exhibited as moments of the distribution function $f(x,\xi,t)$.

$$\rho(x,t) = \int f(x,\xi,t)\, d\xi \qquad \text{(zeroth moment)} \tag{1.7}$$

$$m(x,t) = \int \xi\, f(x,\xi,t)\, d\xi \qquad \text{(first moment)} \tag{1.8}$$

Definition: A weak solution of equations (1.5)-(1.6) is a scalar function $\rho(x,t)$ and a vector function $m(x,t)$ such that for all scalar function $\psi(x,t)$ and vector function $\phi(x,t)$ smooth with compact support in $\mathbb{R}^2\times[0,T]$ such that

$$(1.9)\qquad \int_0^T \int \left\{ \rho \frac{\partial \psi}{\partial t} + m \nabla \psi \right\} dx\, dt = -\int \rho(x,0)\, \psi(x,0)\, dx$$

$$(1.10)\qquad \int_0^T \int \left\{ m \frac{\partial \phi}{\partial t} + \frac{1}{\rho} \sum_{i,j=1}^{2} \left(\frac{\partial \phi_i}{\partial x_j} m_i m_j \right) + p \nabla \phi \right\} dx\, dt = -\int m(x,0)\, \phi(x,0)\, dx$$

Equations (1.9) and (1.10) are solved, approximately, by the kinetic model.

The idea of introducing the phase space (x,ξ) and the distribution function $f(x,\xi,t)$ for the solution of the system (1.5)-(1.6) with $p=F(\rho)$ is such that a simple evolution in time of $f(x,\xi,t)$ will result in approximation to the system to be computed.

The evolution of $f(x,\xi,t)$ is determined by time-cycles of length Δt (not necessarily be constant). At the beginning of the cycle $f(x,\xi,j\Delta t)$ takes a normal form which is specified later. The normal form depends on $\rho(x,j\Delta t)$ and $m(x,j\Delta t)$. For $j\Delta t \le t \le (j+1)\Delta t$, $f(x,\xi,t)$ evolves by free streaming, i.e.

$$(1.11)\qquad f(x,\xi,t) = f(x-\xi\tau,\xi,j\Delta t)$$

where $\tau = t - j\Delta t$. Then equations (1.7) and (1.8) are used to define $\rho(x,t)$ and $m(x,t)$. When t approaches $(j+1)\Delta t$ from below, an intermidiate $\hat{f}$ is determined by

$$(1.12)\qquad \hat{f}(x,\xi,(j+1)\Delta t) = f(x-\xi\Delta t,\xi,j\Delta t)$$

Then $\rho(x,(j+1)\Delta t)$ and $m(x,(j+1)\Delta t)$ are again defined by (1.7) and (1.8) with change of f to $\hat{f}$. Then a new cycle begins, i.e. $f(x,\xi,(j+1)\Delta t)$ takes again the normal form dependent on

$\rho(x,(j+1)\Delta t)$ and $m(x,(j+1)\Delta t)$.

The differential equation that f satisfies is

$$\frac{\partial f}{\partial t} + \sum_i \xi_i \frac{\partial f}{\partial x_i} = 0 \tag{1.13}$$

which is the Boltzmann equation without the collision term. Now, let us state the following theorem. The proof is given in [3].

Theorem 1.1: Let $f(x,\xi,t)$ be integrable with compact support in ξ; $x \in \mathbb{R}^2$. Let us assume, at discrete times $j\Delta t$, that $f(x,\xi,t)$ is changed, so that the total mass and momentum (equations (1.7) and (1.8)) are conserved. Then assuming (1.11), there exists a sub domain $\Omega(\Delta t)$:

$$\Omega(\Delta t) = \left\{x \mid x-\xi\Delta t \in \Omega \ \forall\ \xi \text{ in support of } f\right\}$$

where the equations

$$\frac{\partial}{\partial t}\int f(x,\xi,t)\, d\xi + \sum_i \frac{\partial}{\partial x_i}\int \xi_i\, f(x,\xi,t)\, d\xi = 0 \tag{1.14}$$

$$\frac{\partial}{\partial t}\int \xi_j\, f(x,\xi,t)\, d\xi + \sum_i \frac{\partial}{\partial x_i}\int \xi_i\xi_j\, f(x,\xi,t)\, d\xi = 0 \tag{1.15}$$

are fulfilled in a weak sense. ∎

By equations (1.7) and (1.8), equation (1.14) is equivalent to the continuity equation (1.5). Equation (1.15) is not, in general, equivalent to the momentum equation (1.6).

It is shown in [4] that it is possible to choose $f(x,\xi,j\Delta t)$ so that the momentum equation will be satisfied for $t=j\Delta t$, provided that m_j and $\int \xi_i \xi_j f d\xi$ are differentiable. Such f is said to be in the normal form. The normal form of $f(x,\xi,t)$ is constructed by a generating function $g(|\xi|)$ which is in general a thermodynamic function. As such it has to be dependent on other thermodynamic variables, like ρ,p,S etc. The normal form of $f(x,\xi,j\Delta t)$ is given by

$$(1.16)\quad f(x,\xi,j\Delta t) = \begin{cases} g(|\xi-u(x,j\Delta t)|) & |\xi-u(x,j\Delta t)| \le \sqrt{2}c(x,j\Delta t) \\ 0 & |\xi-u(x,j\Delta t)| > \sqrt{2}c(x,j\Delta t) \end{cases}$$

where c is the local speed of sound.

In $\mathbb{R}^2$, for the equation of state

$$(1.17)\qquad p = A\,\rho^{\gamma}$$

where A is in general a function of entropy, in our case it is a constant, and the generating function g is

$$(1.18)\quad g(\omega) = (1/2\pi)\,(A.2\gamma)^{-1/(\gamma-1)}\,(2/(\gamma-1))\,\omega^{(4-2\gamma)/(\gamma-1)}$$

where ω, being multiple of speed of sound, is also a thermodynamic variable given by

$$(1.19)\quad \omega^2 = 2c^2 = 2\,\frac{\partial p}{\partial \rho}$$

For the detailed derivation of g refer [5].

In this paper we have considered an ideal gas with $\gamma=7/5$ (Air) in equation (1.17). In the rest, we have carried out the two-dimensional computation.

2. Analytical Computation Of Basic Flux Functions

The domain is divided into rectangular cells. Let the cell (i,j) be bounded by $x_1=x_1^{(i)}$, $x_1-x_1^{(i+1)}$ and $x_2=x_2^{(j)}$, $x_2=x_2^{(j+1)}$. Denote this by C_{ij}. Let ρ_{ij} and m_{ij} denote the total mass and momentum respectively in C_{ij}. The algorithm consists of the updating of the total mass and total momentum in the respective cells.

In this case, we have to consider as the donor view point by which the total mass and momentum that for t=0 in C_{ij} determines the same in C_{kl} at $t=\Delta t$. This is nothing but the transport of mass and momentum from C_{ij} to C_{kl}. The algorithm is exhibited by showing how to compute $\rho_{ij}(\Delta t)$ and $m_{ij}(\Delta t)$ provided $\rho_{ij}(0)$ and $m_{ij}(0)$ are known. The density ρ is assumed to be constant in each cell, also the velocity $u=m/\rho$ is assumed to be constant in each cell. Discontinuities are admissible at the cell's boundaries. This way $c(x,0)$ and $u(x,0)$ are known. These determine $f(x,\xi,0)$ which determines, by kinetic model $f(x,\xi,\Delta t)$.

The velocity ξ of a molecule located at x can be decomposed into $\xi=u(x,0)+(\xi-u(x,0))$. We are considering here the first movement of C_{ij} by $\Delta t\cdot u(x,0)$. Since $u(x,0)$ is assumed to be constant in each cell, a rectangle cell C_{ij} will

move to another rectangle U_{ij}. And then the molecule will be dispersed by $\Delta t\cdot(\xi-u(x,0))$ where $|\xi-u(x,0)|\le\sqrt{2}c(x,0)$.

The purpose here is to determine the total mass and total momentum in each cell. In order to do so, it is enough to compute these in half space (say $x_1\ge x_1^{(i)}$)(called side flux) and the quarter space (say $x_1\ge x_1^{(i)}$, $x_2\ge x_2^{(j)}$) (called corner flux) which in turn serves as basic flux functions. We shall see in the next section how the flux terms are computed using these functions.

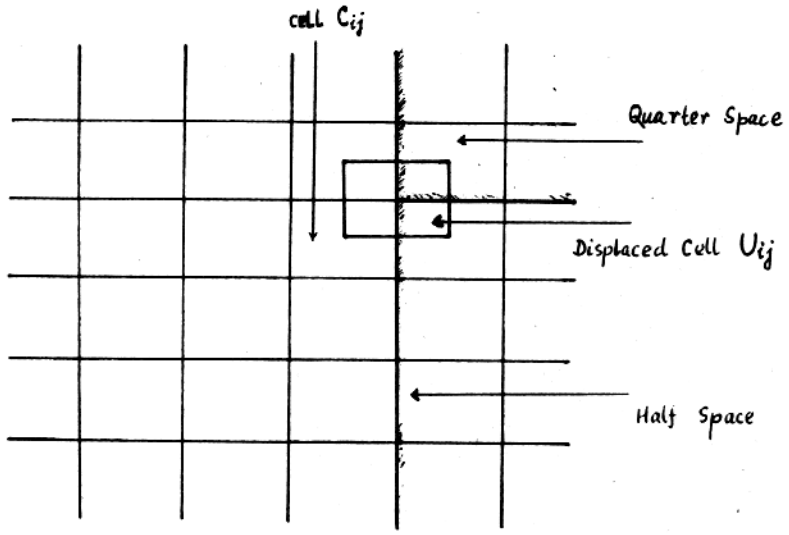

Fig.2.1 Half Space and Quarter Space

Let us denote these functions by $SF_{m,n}$ and $CF_{m,n}$ respectively, where

m,n

0,0 —— mass

1,0 —— x_1-momentum

0,1 —— x_2-momentum.

In clear terms, the basic side flux function $SF_{m,n}(a)$ is defined as the total flux that emanates from the region $x_1^{(i)}=0 \le x_1 \le a$ $(a \ge 0)$ crossing the line $x_1=0$ as shown in figure 2.2.

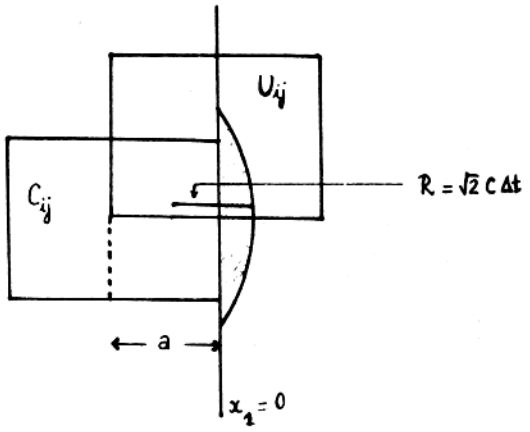

Fig.2.2 Integration Domain for the Side Flux

Also notice that for a two dimensional problem, the integrals involved are four dimensional.

(a) Mass side flux computation:

$$(2.1)\qquad SF_{o,o}(a) = \int\int_{\substack{x_1 \geq x_1^{(i)} \\ x-\xi\Delta t \in C_{ij}}} f(x,\xi,\Delta t)\, d\xi\, dx$$

$$= \int\int_{\substack{x_1 \geq x_1^{(i)} \\ x-\xi\Delta t \in C_{ij}}} f(x-\xi\Delta t,\xi,0)\, d\xi\, dx \qquad \text{(by eqn.(1.11))}$$

$$\overset{x-\xi\Delta t=y}{=} \int\int_{\substack{y_1+\xi_1\Delta t \geq 0 \\ y \in C_{ij}}} f(y,\xi,0)\, d\xi\, dy$$

$$= \int\int_{\substack{y_1+\xi_1\Delta t \geq 0 \\ |\xi-u_{ij}| \leq \sqrt{2}\, c_{ij} \\ y \in C_{ij}}} g(|\xi-u_{ij}|)\, d\xi\, dy \qquad \text{(by eqn.(1.16))}$$

$$\overset{\xi-u_{ij}=\eta}{=} \int\int_{\substack{y_1+(\eta_1+u_{ij}^{(i)})\Delta t \geq 0 \\ y \in C_{ij} \\ |\eta| \leq \sqrt{2}\, c_{ij}}} g(|\eta|)\, d\eta\, dy$$

We have performed firstly the η-integration and then the y-integration. In our case, it is clearly seen that the thermodynamic function

$$g(|\eta|) = 5/2\pi\ (A\times 2.8)^{-5/2}\ |\eta|^3 \tag{2.2}$$

by taking γ=1.4 in eqn.(1.18)

So,

$$SF_{o,o}(a) = \int (\text{velocity integration } (VIS_{mass}))\ dy \tag{2.3}$$

where

$$VIS_{mass} = \int g(|\eta|)\ d\eta \tag{2.4}$$

$$= K \int\int |\eta|^3\ d\eta_1\ d\eta_2$$

where $K=5/2\pi\ (A\times 2.8)^{-5/2}$ and $\eta^2 = \eta_1^2 + \eta_2^2$.

We have carried out the integration (2.4) by polar coordinates (see fig.2.3).

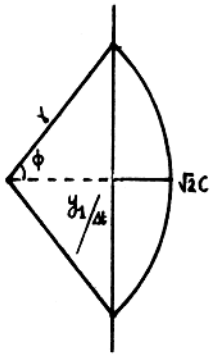

Fig.2.3 Velocity Integration for the Side Flux

which gives

$$(2.5) \qquad VIS_{mass} = K \int_{y_1/\Delta t}^{\sqrt{2}c} (2\phi)\ r^3\ r\ dr$$

where ϕ-integration is just 2ϕ and $\phi = \arccos\frac{(y_1/\Delta t)}{r}$.

Remember that C is c(x,0), the local speed of sound.

$$(2.6) \qquad VIS_{mass} = 2K \int_{y_1/\Delta t}^{\sqrt{2}c} r^4\ \phi\ dr$$

which leads to

$$(2.7) \qquad VIS_{mass} = \frac{2K}{5\Delta t^5} \left\{ R^5 \arccos(y_1/R) - (y_1/4)\ R^3 \sqrt{R^2-y_1^2} \right.$$

$$\left. - \frac{3Ry_1^3}{8} \sqrt{R^2-y_1^2} - (3/8)\ y_1^5 \log\left(\frac{R+\sqrt{R^2-y_1^2}}{y_1} \right) \right\}$$

where $R=\sqrt{2}c\Delta t$.

Therefore

$$(2.8) \qquad SF_{o,o} = \int \int VIS_{mass}\ dy_1\ dy_2$$

where the limits are: $0 \le y_1 \le a$ and $0 \le y_2 \le \Delta y(=\Delta x_2)$, but we have taken $\Delta y=1$. After a lengthy calculation we have

$$(2.9)\quad SF_{o,o}(a) = (\rho R/\pi)\Big\{\sigma \arccos\sigma - (\sigma^6/16)\log\Big(\frac{1+\sqrt{1-\sigma^2}}{\sigma}\Big)$$

$$- \frac{3}{40}(1-\sigma^2)^{5/2} + \frac{5}{24}(1-\sigma^2)^{3/2} + \frac{\sqrt{1-\sigma^2}}{10}$$

$$\times\Big(\sigma^4/8 + \sigma^2/6 - 2g/3\Big) + 5/6\Big\}$$

where $\sigma = a/R$. When $\sigma > 1$, $SF_{o,o}(\sigma) = SF_{o,o}(1)$.

(b) Momentum side flux computation:

$$(2.10)\qquad SF_{m,n}(a) = \int\int_{\substack{y_1+\xi_1\Delta t\geq 0 \\ y\in C_{ij}}} \xi_k\, f(y,\xi,0)\, d\xi\, dy$$

$$= \int\int_{\substack{y_1+\xi_1\Delta t\geq 0 \\ |\xi-u_{ij}|\leq \sqrt{2}c_{ij} \\ y\in C_{ij}}} \xi_k\, g(|\xi - u_{ij}|\, d\xi\, dy$$

$$\underset{=}{\xi-u_{ij}=\eta} \int\int_{\substack{y_1+(\eta_1+u_{ij}^{(1)})\Delta t\geq 0 \\ |\eta|\leq\sqrt{2}c_{ij} \\ y\in C_{ij}}} (\eta_k + u_{ij}^{(k)})g(|\eta|)\, d\eta\, dy$$

$$= \int\int_{\substack{y_1+(\eta_1+u_{ij}^{(1)})\Delta t\geq 0 \\ |\eta|\leq\sqrt{2}c_{ij} \\ y\in C_{ij}}} \eta_k\, g(|\eta|)\, d\eta\, dy + u_{ij}^{(k)} \int\int_{\substack{y_1+(\eta_1+u_{ij}^{(1)})\Delta t\geq 0 \\ |\eta|\leq\sqrt{2}c_{ij} \\ y\in C_{ij}}} g(|\eta|)\, d\eta\, dy$$

The second term in above is nothing but the mass side flux function times the flow velocity. Proceeding as in the above way (i.e. case (a)) we will end up with the velocity integration of first term of (2.10), reading as

$$(2.11a)\quad VIS_{x_1\text{-mom}} = \frac{2K}{\Delta t^6}\left\{ \frac{R^3}{6}\left(R^2-y_1^2\right)^{3/2} + \frac{R}{8}\, y_1^2\left(R^2-y_1^2\right)^{3/2} + -\frac{R}{16}\, y_1^4\sqrt{R^2-y_1^2} - \frac{y_1^6}{16}\log\left(\frac{R+\sqrt{R^2-y_1^2}}{y_1}\right)\right\}$$

and

$$(2.11b)\quad VIS_{x_2\text{-mom}} = 0$$

Further computation finally leads to $SF_{1,0}(a)$ and $SF_{0,1}(a)$ given by

$$(2.12a)\quad SF_{1,0}(a) = \frac{5\sqrt{2}\rho cR}{16\pi}\left\{\frac{8}{7}\arcsin\sigma - \frac{\sigma^7}{7}\log\left(\frac{1+\sqrt{1-\sigma^2}}{\sigma}\right) - \frac{\sigma}{3}(1-\sigma^2)^{5/2} + \frac{\sigma}{7}(1-\sigma^2)^{3/2}\left(\frac{75}{16}-\frac{\sigma^2}{3}\right)\right.$$

$$+ \sigma\sqrt{1-\sigma^2}\left(\frac{\sigma^4}{7} - \frac{5\sigma^2}{112} + \frac{19}{16}\right)\Big\} + u^{(1)}SF_{o,o}(a)$$

and

(2.12b) $\quad SF_{o,1}(a) = u^{(2)}SF_{o,o}(a)$

where $\sigma = a/R$. When $\sigma > R$ $SF_{m,n}(\sigma) = SF_{m,n}(1)$.

(c) Mass corner flux computation:

The starting part is same as we have done in the side flux computation. The integration domain for the corner flux is given in fig.2.4.

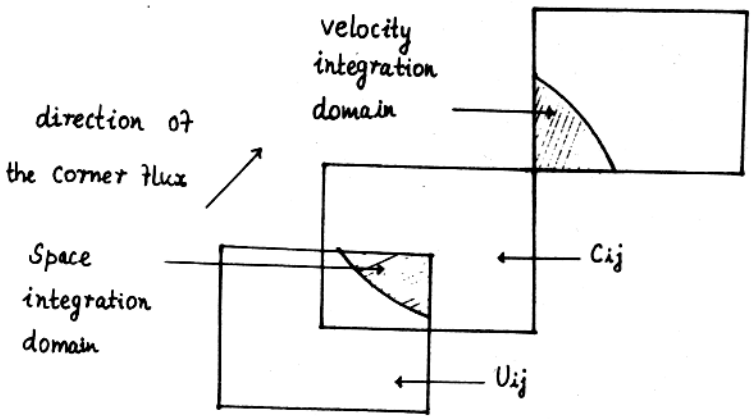

Fig.2.4 Integration Domain for the Corner Flux

Here also we are doing the velocity integration first and then follows the space integration. By polar coordinates for the velocity integration (see fig.2.5).

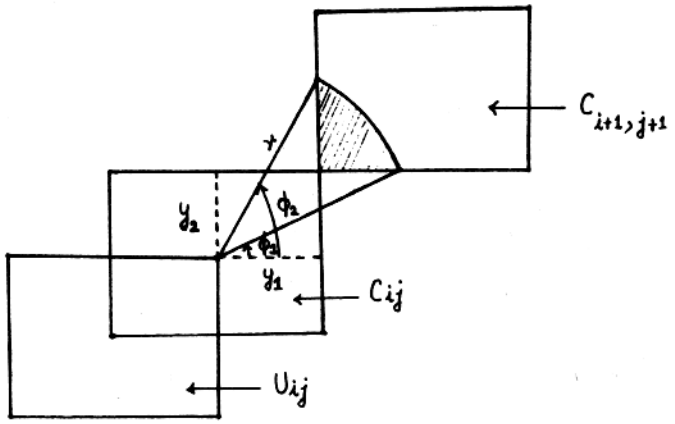

Fig.2.5 Velocity Integration for the Corner Flux

We have

$$(2.13)\quad VIC_{mass} = K \int_{L}^{\sqrt{2}c} \int_{\phi_1}^{\phi_2} r^3 \, r \, d\phi \, dr$$

where $L = \left(\sqrt{y_1^2 + y_2^2}\right)/\Delta t$, $\phi_1 = \arcsin\frac{(y_2/\Delta t)}{r}$

and

$\phi_2 = \arccos\frac{(y_1/\Delta t)}{r}$. After integration

$$(2.14)\quad VIC_{mass} = \frac{K}{5\Delta t^5}\left\{R^5\left(\arccos\frac{y_1}{R} + \arccos\frac{y_2}{R}\right)\right.$$

$$- (R^3/4)\left(y_1\sqrt{R^2 - y_1^2} + y_2\sqrt{R^2 - y_2^2}\right)$$

$$- (3R/8)\left(y_1^3\sqrt{R^2 - y_1^2} + y_2^3\sqrt{R^2 - y_2^2}\right)$$

$$- (3/8)\left(y_1^5\log\left(R+\sqrt{R^2-y_1^2}\right) + y_2^5\log\left(R+\sqrt{R^2-y_2^2}\right)\right)$$

$$+(7/8)y_1y_2(y_1^2+y_2^2)^{3/2} + (3/8)\left(y_1^5\log\left(y_2+\sqrt{y_1^2+y_2^2}\right)\right.$$

$$\left.\left. + y_2^5\log\left(y_1+\sqrt{y_1^2+y_2^2}\right)\right) - (\pi/2)R^5\right\}$$

For the space integration, we have the following figure:

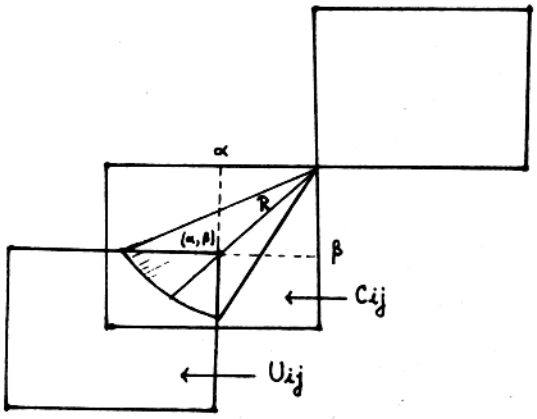

Fig.2.6 Space Integration for the Corner Flux

where $\alpha = u^{(1)}\Delta t$ and $\beta = u^{(2)}\Delta t$.

So it is clear that the range for y_1 is α to $\sqrt{R^2-\beta^2}$ and that for y_2 is β to $\sqrt{R^2-y_1^2}$. After a very lengthy calculation, the mass corner flux is given by

$$(2.15)\quad CF_{o,o}(\alpha,\beta) = (\rho R^2/2\pi)\Big\{\sigma\theta(\arccos\sigma - \arcsin\theta)$$

$$+ (\theta\sigma^6/16)\log\left(\frac{\theta+\sqrt{\sigma^2+\theta^2}}{1+\sqrt{1-\sigma^2}}\right) + (\sigma\theta^6/16)\log\left(\frac{\sigma+\sqrt{\sigma^2+\theta^2}}{1+\sqrt{1-\theta^2}}\right)$$

$$- \theta\sqrt{1-\sigma^2}\left(\frac{\sigma^4}{16} + \frac{\sigma^2}{24} + \frac{5}{6}\right) - \sigma\sqrt{1-\theta^2}\left(\frac{\theta^4}{16} + \frac{\theta^2}{24} + \frac{5}{6}\right)$$

$$+ \frac{\sigma^2+\theta^2}{2} + \sqrt{\sigma^2+\theta^2}\left(\frac{25\sigma^4\theta^2}{336} + \frac{25\theta^4\sigma^2}{336} - \frac{\theta^6}{42} - \frac{\sigma^6}{42}\right) + \frac{5}{14}\Big\}$$

$$= CF_{o,o}(\beta,\alpha)$$

where $\sigma = \alpha/R$ and $\theta = \beta/R$, and when $\sqrt{\sigma^2+\theta^2} > 1$ $CF_{o,o}(\alpha,\beta)=0$, which can be realized easily, i.e. no corner flux contribution.

(d) Momentum corner flux computation:

A similar computation as in the mass corner flux and as in the momentum side flux leads to the following:

$$(2.16a)\quad VIC_{x_1\text{-mom}}(y_1,y_2) = (K/\Delta t^6)\Big\{(R^3/6)(R^2-y_1^2)^{3/2} + \frac{y_1^2}{8}R\,(R^2-y_1^2)^{3/2} + \frac{y_1^4}{16}R\sqrt{R^2-y_1^2} - \frac{y_1^2}{16}\log\left(R+\sqrt{R^2-y_1^2}\right) - \frac{y_2^3}{6}(y_1^2+y_2^2)^{3/2} - \frac{y_1^2 y_2^3}{8}\sqrt{y_1^2+y_2^2} - \frac{y_1^4}{16}y_2\sqrt{y_1^2+y_2^2} + \frac{y_1^6}{16}\log\left(y_2+\sqrt{y_1^2+y_2^2}\right) - \frac{y_2}{5}R^5 + \frac{y_2}{5}\left(y_1^2+y_2^2\right)^{5/2}\Big\}$$

$$(2.16b)\quad VIC_{x_2\text{-mom}}(y_1,y_2) = VIC_{x_1\text{-mom}}(y_2,y_1)$$

and

$$(2.17a)\quad CF_{1,0}(\alpha,\beta) = \frac{5\rho c R^2}{\sqrt{2\pi}}\Big\{\frac{\theta}{14}(\arcsin\sigma - \arccos\theta) + \frac{\sigma^7\theta}{112}\log\left(\frac{\theta+\sqrt{\sigma^2+\theta^2}}{1+\sqrt{1-\sigma^2}}\right) + \frac{\theta^8}{896}\log\left(\frac{\sigma+\sqrt{\sigma^2+\theta^2}}{1+\sqrt{1-\theta^2}}\right) + \sqrt{\sigma^2+\theta^2}\left(\frac{7\sigma\theta^6}{1920} + \frac{3\sigma^3\theta^4}{448} + \frac{\sigma^5\theta^2}{105} - \frac{\sigma^7}{280}\right) + \sqrt{1-\theta^2}\left(-\frac{\theta^6}{896} - \frac{\theta^4}{1344} + \frac{11\theta^2}{336} + \frac{1}{24}\right) + \sqrt{1-\sigma^2}\left(\frac{2\sigma\theta}{21} - \frac{\sigma^3\theta}{168} - \frac{\sigma^5\theta}{112}\right) - \sigma\left(\frac{\theta^2}{10} + \frac{1}{14}\right)$$

$$+ \frac{\sigma^3}{30} \Big\} + u^{(1)} CF_{0,0}(\alpha,\beta)$$

(2.17b) $$CF_{0,1}(\alpha,\beta) = CF^{I}_{1,0}(\beta,\alpha) + u^{(2)} CF_{0,0}(\alpha,\beta)$$

where $CF^{I}_{1,0}$ is the first term of $CF_{1,0}(\alpha,\beta)$ and when $\sqrt{\sigma^2+\theta^2}>1$, $CF_{1,0}(\alpha,\beta) = CF_{0,1}(\alpha,\beta) = 0$.

3. The Organization Of Flux Computation

The basic assumptions that we made here are:

(1) The fluid is an ideal gas having $\gamma = 1.4$

(2) The time step is limited by

$$(|u^{(1)}| + \sqrt{2}c)\Delta t < \Delta x_1$$

$$(|u^{(2)}| + \sqrt{2}c)\Delta t < \Delta x_2$$

(3) The flow field ρ, u, c is considered to be piecewise constant in each cell.

(4) The cells are rectangular.

The assumption (2) is nothing but the CFL condition which keeps the consideration of the nearest neighbours for the mass and momentum exchange. Figure 3.1 shows the consideration of the cell C_{ij} and its eight neighbours.

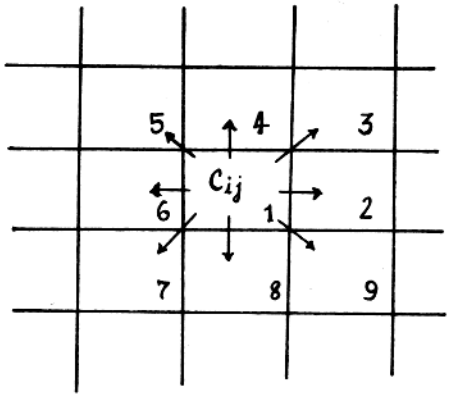

Fig.3.1 Cell C_{ij} with Outgoing Flux

Let $f_{ij}(k,\ell)$ be the flux from C_{ij} to its neighbours such that

$f_{ij}(k,1)$ - mass flux

$f_{ij}(k,2)$ - x_1-momentum flux

$f_{ij}(k,3)$ - x_2-momentum flux

where ℓ = 1,2,3, k takes the values 1,2,..,9 and $f_{ij}(1,1)$ is the mass/momentum flux remaining in the cell C_{ij}.

The evaluation of $f_{ij}(k,\ell)$ from the basic flux functions $SF_{m,n}(a)$ and $CF_{m,n}(\alpha,\beta)$ is given as follows: Let us consider a general case (fig.3.2) where the displaced cell U_{ij} has moved through time step Δt so that the point $(x_1,x_2) = (0,0)$ is at $(\alpha = u^{(1)}\Delta t, \beta = u^{(2)}\Delta t)$.

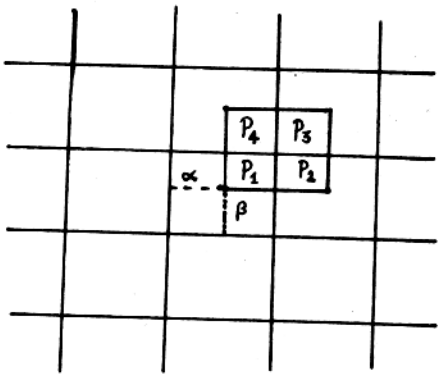

Fig.3.2 Sub-domains of the Displaced Cell

Here P_1,P_2,P_3,P_4 are the subdomains of the displaced cell. For example, the flux contribution to the part P_3 is the sum of the four contributions each corresponding to one of the four parts of U_{ij}, which involves the computation of $SF_{m,n}(a)$ and $CF_{m,n}(\alpha,\beta)$ in the appropriate combinations.

Now, let us look into the computation of $f_{ij}(2,1)$, i.e. the mass flux from cell 1 to cell 2 (fig.3.3), using the basic flux functions with the above set up.

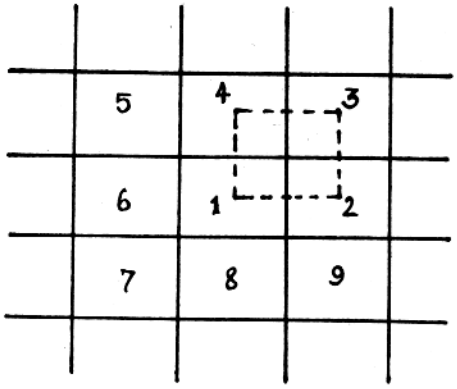

Fig.3.3 Computation of Flux Terms when $u^{(1)}$ and $u^{(2)} > 0$

By refering fig.3.3., we have

$$\begin{aligned} f_{ij}(2,1) = {} & f_{ij}(1,1)\alpha(\Delta x_2-\beta) + SF_{o,o}(\Delta x_1-\alpha)(\Delta x_2-\beta) \\ & - cf(1\to3) - cf(1\to9) + cf(4\to2) + sf(3\to2) \\ & - SF_{o,o}(\alpha)(\Delta x_2-\beta) - sf(2\to3) - sf(2\to9) \end{aligned}$$

where $cf(\ell_1\to\ell_2)$ is the corner flux from cell ℓ_1 to cell ℓ_2 and $sf(\ell_1\to\ell_2)$ is for the side flux, such that

$$\begin{aligned} cf(1\to3) = {} & CF_{o,o}(0,0) - CF_{o,o}(0,\Delta x_2-\beta) - CF_{o,o}(\Delta x_1-\alpha,\beta) \\ & + CF_{o,o}(\Delta x_1-\alpha,\Delta x_2-\beta) \end{aligned}$$

$$cf(1\to9) = CF_{o,o}(0,\beta) - CF_{o,o}(\Delta x_1-\alpha,\beta)$$

$$cf(4\to2) = CF_{o,o}(0,0) - CF_{o,o}(0,\beta) - CF_{o,o}(\Delta x_1-\alpha,0)$$

$$+ CF_{o,o}(\Delta x_1-\alpha,\beta)$$

$$sf(3\to2) = SF_{o,o}(\beta)\ \alpha - cf(3\to1)$$

$$sf(2\to3) = SF_{o,o}(\Delta x_2-\beta)\ \alpha - cf(2\to4)$$

$$sf(2\to9) = \left\{SF_{o,o}(1)\ \alpha - SF_{o,o}(\beta)\ \alpha\right\} - cf(2\to8)$$

$$cf(3\to1) = CF_{o,o}(0,0) - CF_{o,o}(\alpha,0) - CF_{o,o}(0,\beta) + CF_{o,o}(\alpha,\beta)$$

$$cf(2\to4) = CF_{o,o}(0,0) - CF_{o,o}(\alpha,0) - CF_{o,o}(0,\Delta x_2-\beta) + CF_{o,o}(\alpha,\Delta x_2-\beta)$$

$$cf(2\to8) = CF_{o,o}(0,\beta) - CF_{o,o}(\alpha,\beta)$$

and $f_{ij}(1,1)$ is the density at every point of the cell C_{ij} at t=0. A similar approach can be carried for other flux neighbours. But when we are dealing with momentum fluxes one has to make attention in the direction of flux and the corresponding components.

For the other cases, i.e., $u^{(1)}<0$, $u^{(2)}>0$; $u^{(1)}$ and $u^{(2)}<0$; $u^{(1)}>0$,$u^{(2)}<0$; it is just the rotation of the moved domain U_{ij} by $\pi/2$ in the anti-clockwise direction. At every time step of computation, we have to update the total mass/momentum in each cell, called flux balance, which is given by

$$(3.1)\quad f_{ij}(1,\ell)_{\,t+\Delta t} = (1/AREA)\left\{f_{ij}(Remaining) + \sum(flux\ in)\right\}$$

where AREA = area of the cell $C_{ij} = \Delta x_1 \Delta x_2$,

$$f_{ij}(\text{Remaining}) = \text{AREA} \times f_{ij}(1,\ell)_t - \sum_{k=2}^{9} f_{ij}(k,\ell)$$

and $\sum$(flux in) can be realized from the following diagram.

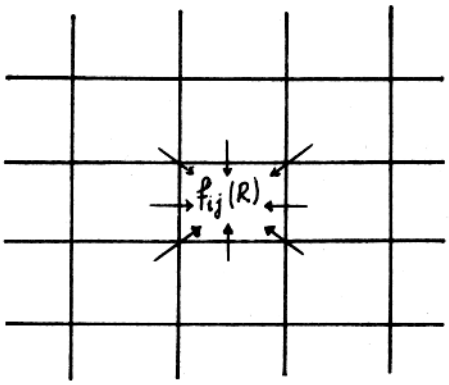

Fig.3.4 Flux In

The above fact in the flux balance is true for the interior flow. But for the boundaries we have considered the specular reflection from the wall, explained in the next section.

4. PRACTICAL CONSIDERATIONS

We have tested here the 1D shock and 2D shock-obstacle interaction problems by numerical computation.

(a) 1D Shock (taking $u^{(2)}=0$)

Here we have taken the interior flow.

(i) *Riemann Problem*: Consider the following figure:

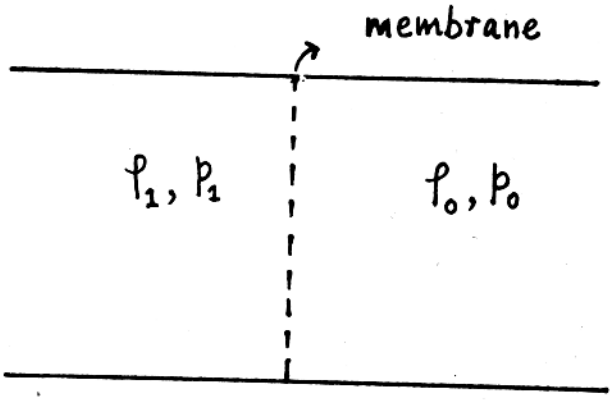

Fig.4.1 Riemann Problem (1D)

The computation is carried out for 350 steps. Figures 4.2-4.6 exhibit the pressure shock, density shock and mach field for different time steps by taking the grid as 360×1.

Univ.-Bibl.
Kaiserslautern

Fig.4.2 1D Shock-Riemann Problem

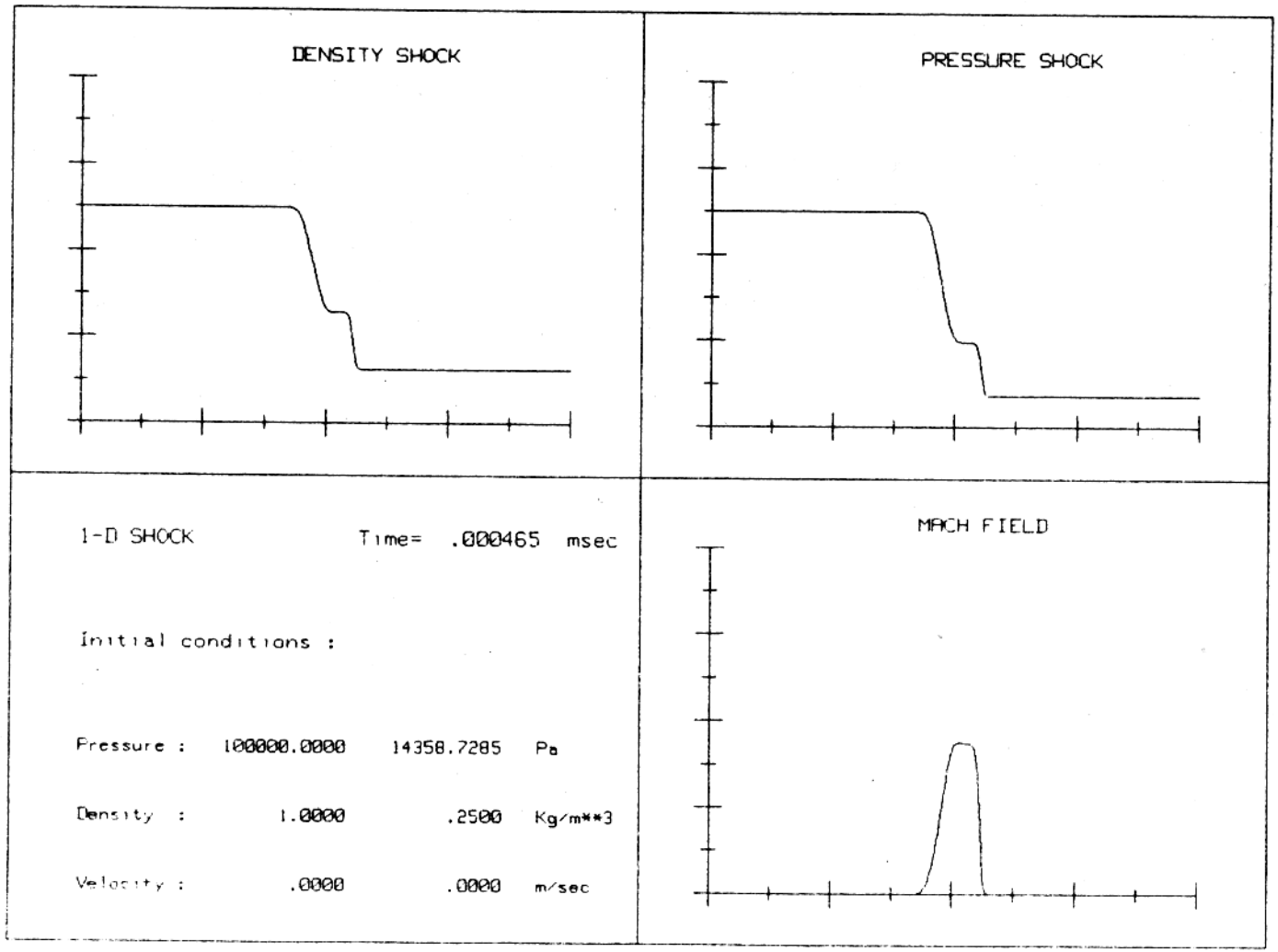

Fig.4.3 1D Shock-Riemann Problem

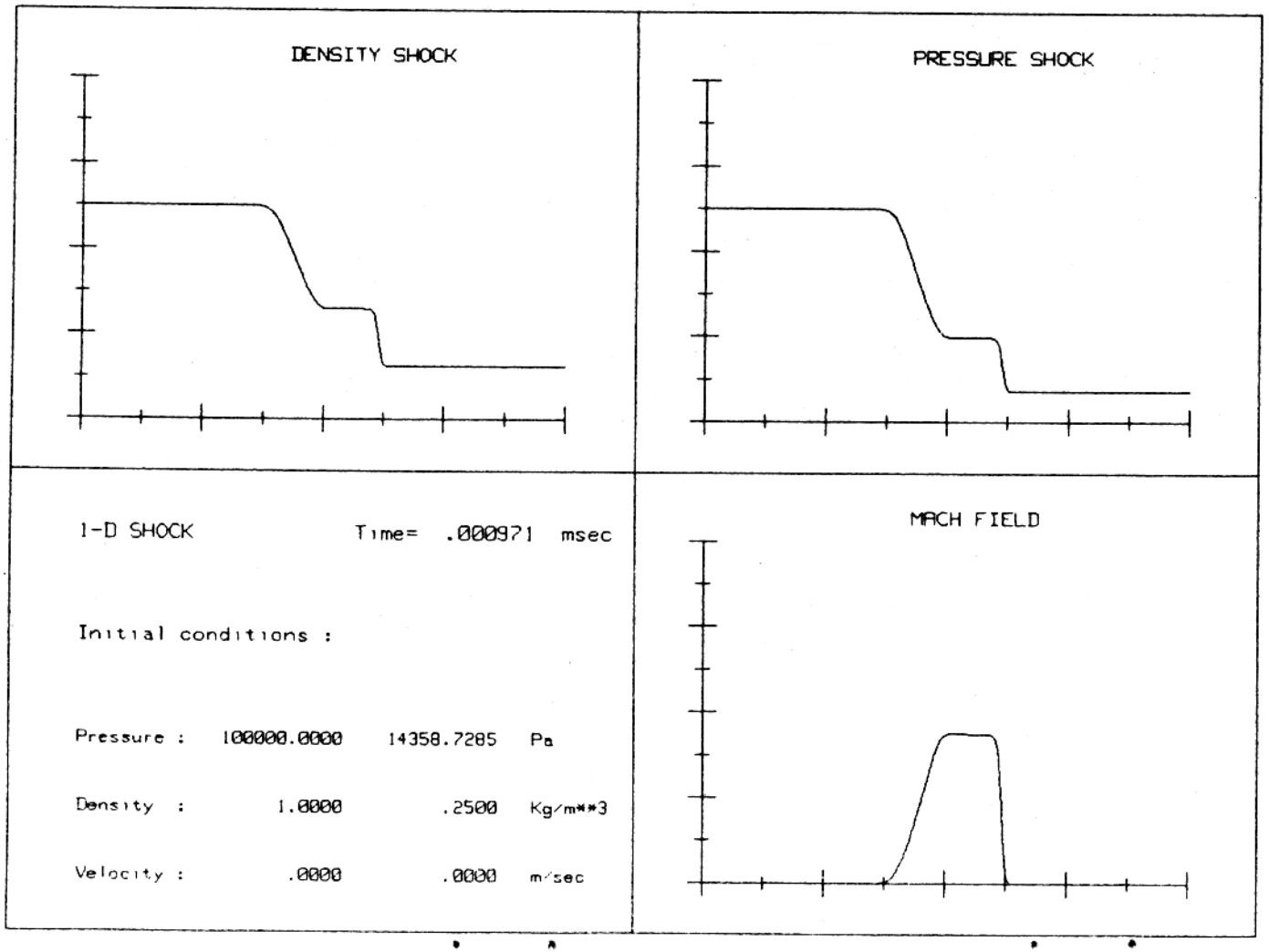

Fig.4.4 1D Shock-Riemann Problem

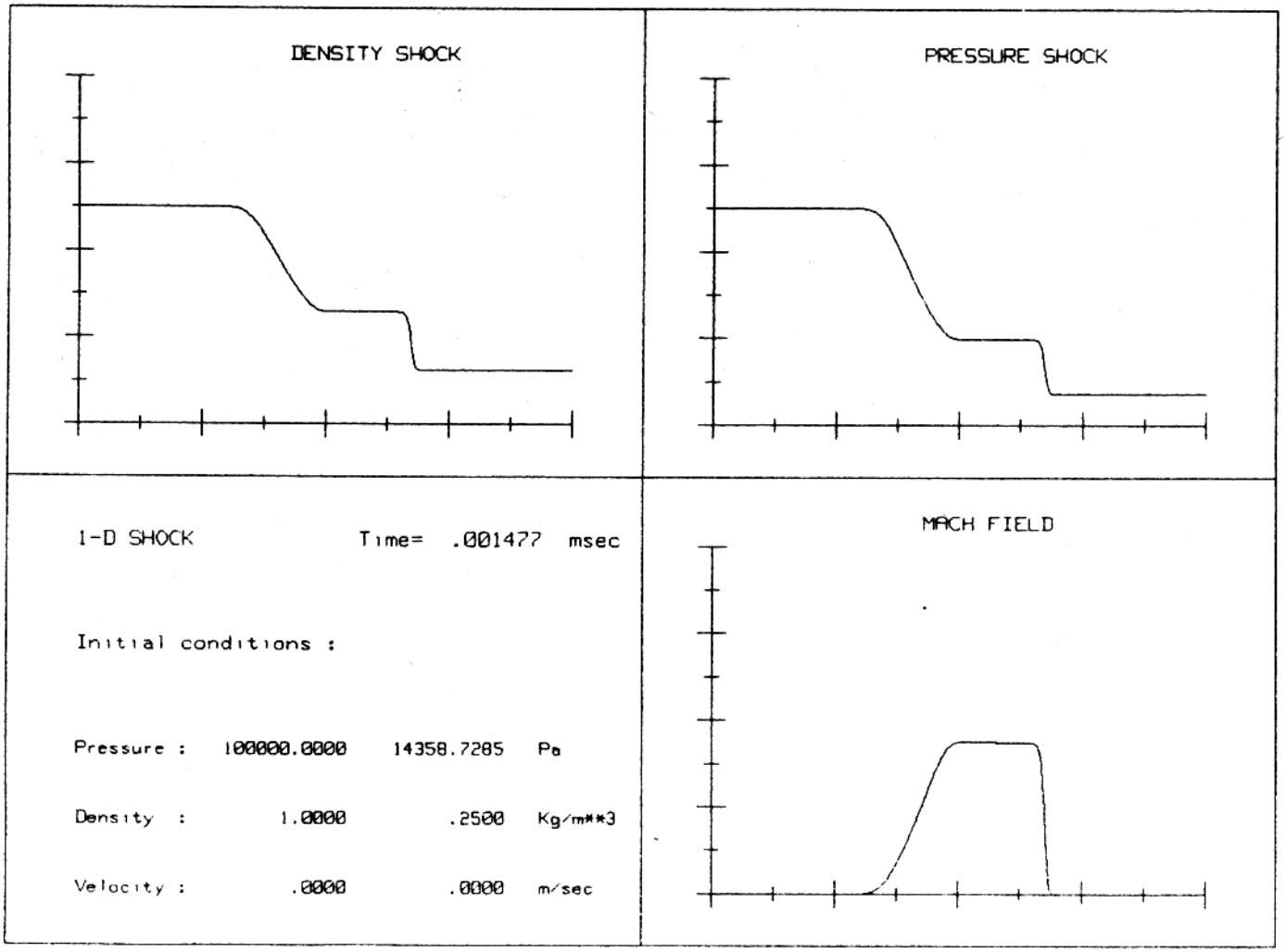

Fig.4.5 1D Shock-Riemann Problem

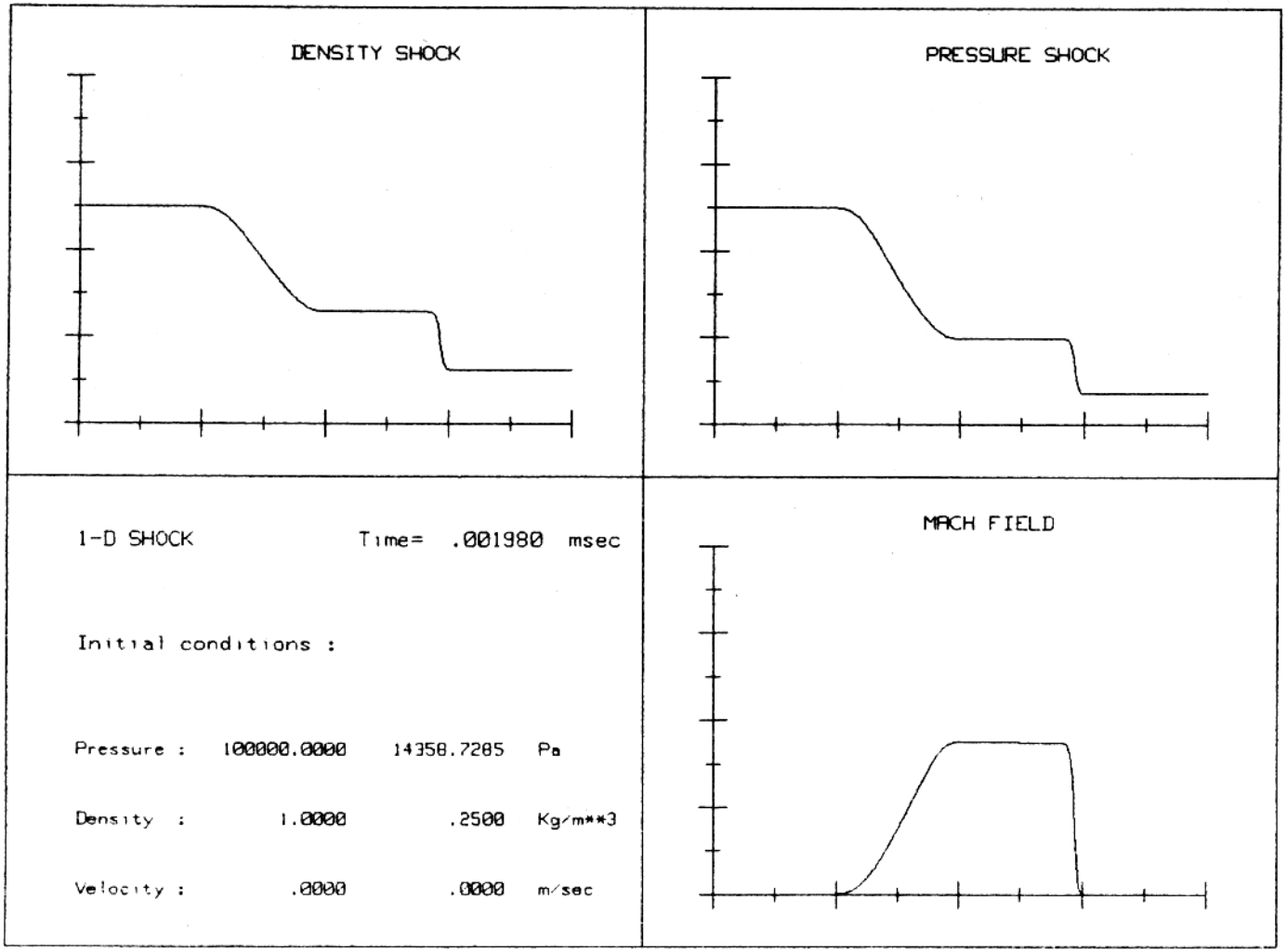

Fig.4.6 1D Shock-Riemann Problem

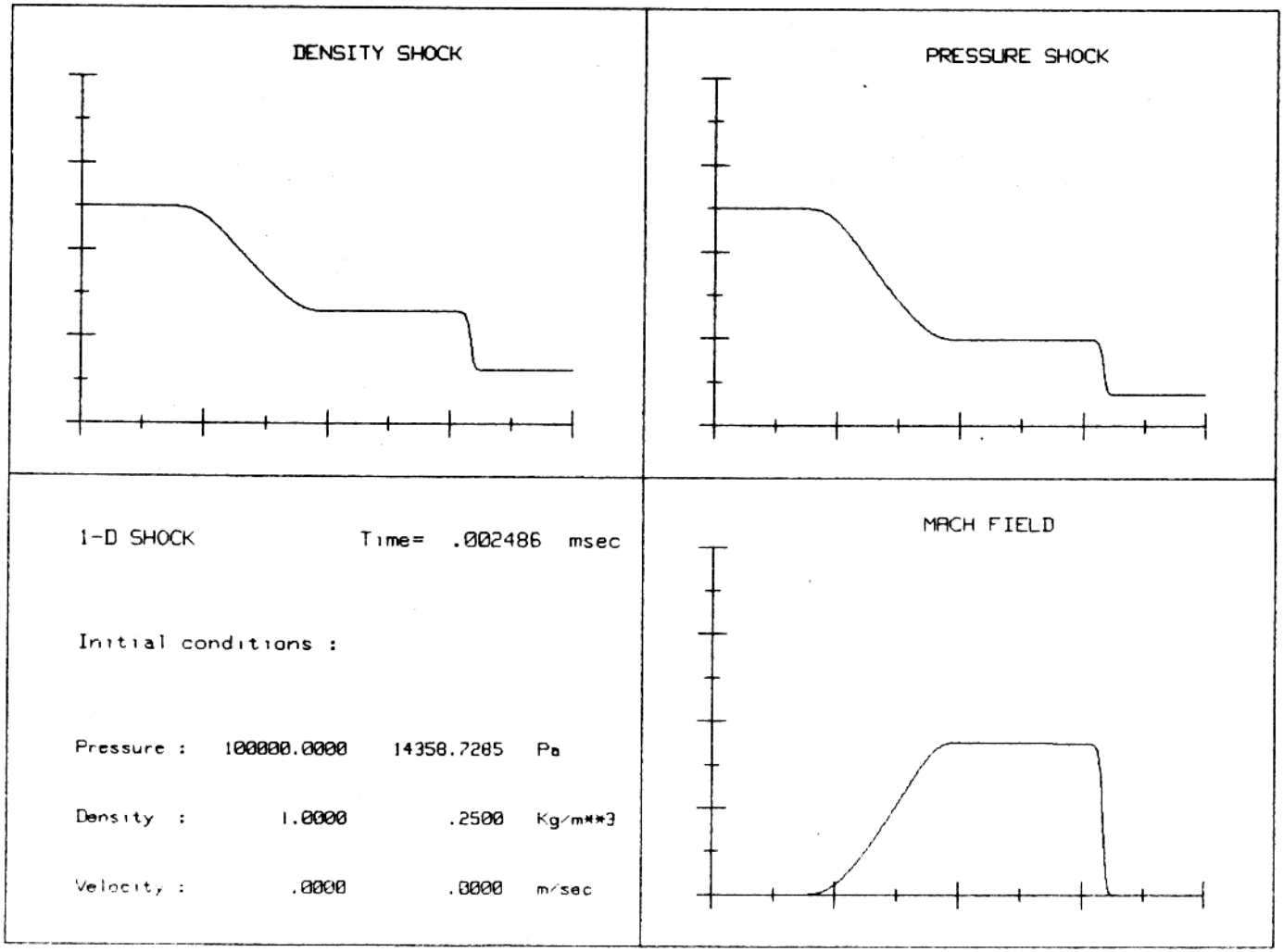

(ii) *Moving Shock Problem*: Consider the following moving shock problem:

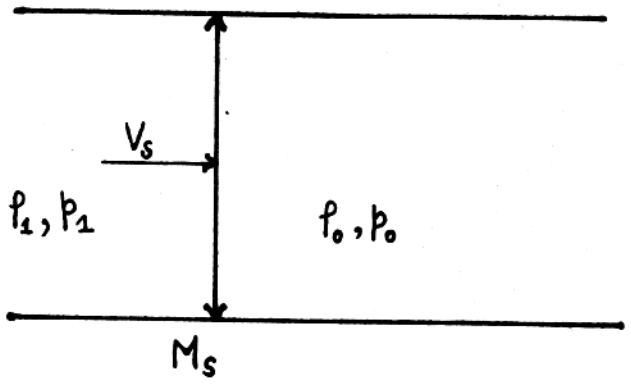

Fig.4.7 Moving Shock Problem (1D)

where V_s is the velocity of the shock, M_s is the shock mach number and the shock starts after 150 cells in our computation. Figures 4.8-4.12 show the development of moving shock for different time levels. The step-like part in these figures are the theoretical shocks. Here, the grid is taken as 360×1 and the shock mach number, M_s is 1.5.

Fig.4.8 1D Shock-Moving Shock Problem

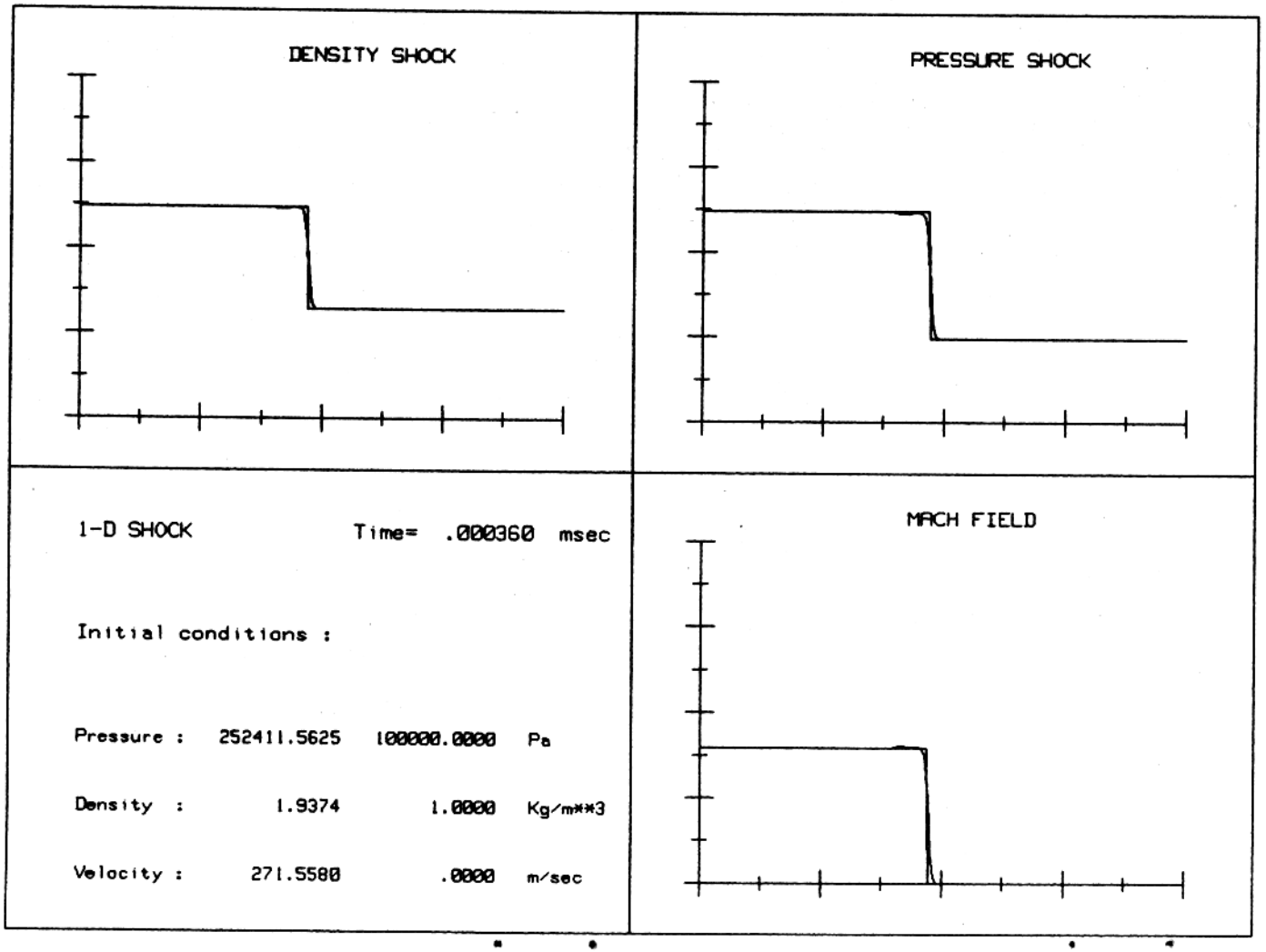

Fig.4.9 1D Shock-Moving Shock Problem

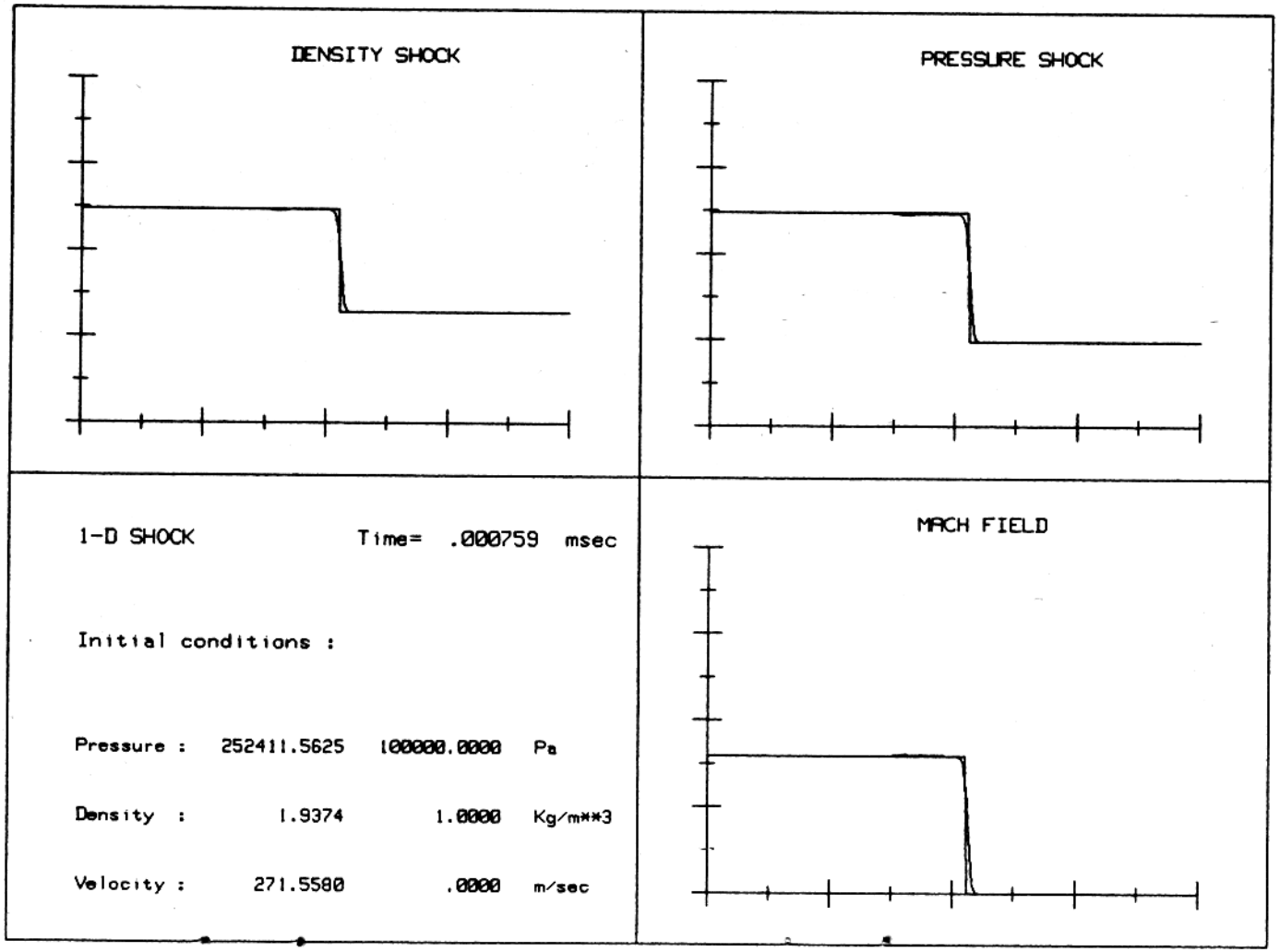

Fig.4.10 1D Shock-Moving Shock Problem

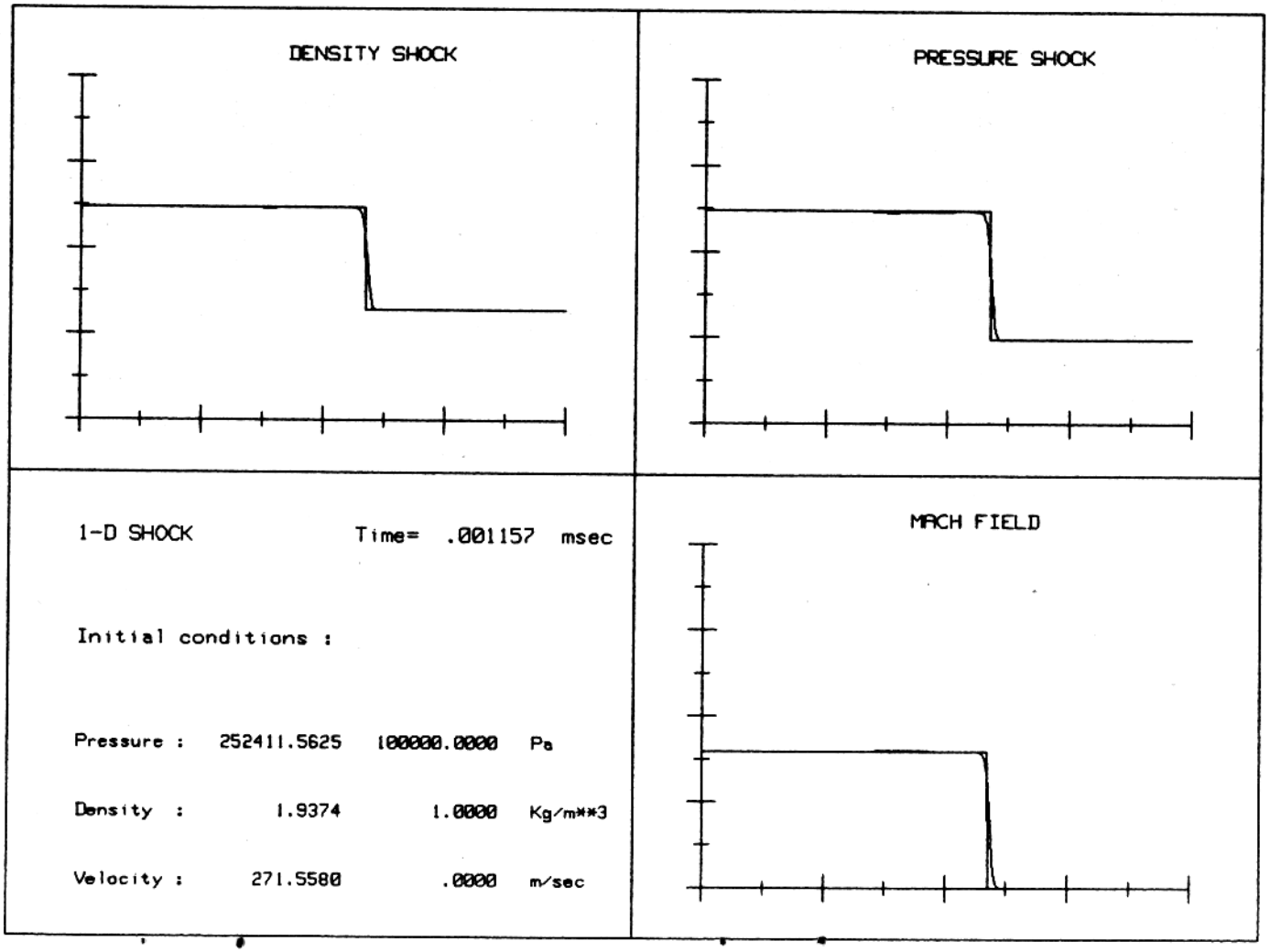

Fig.4.11 1D Shock-Moving Shock Problem

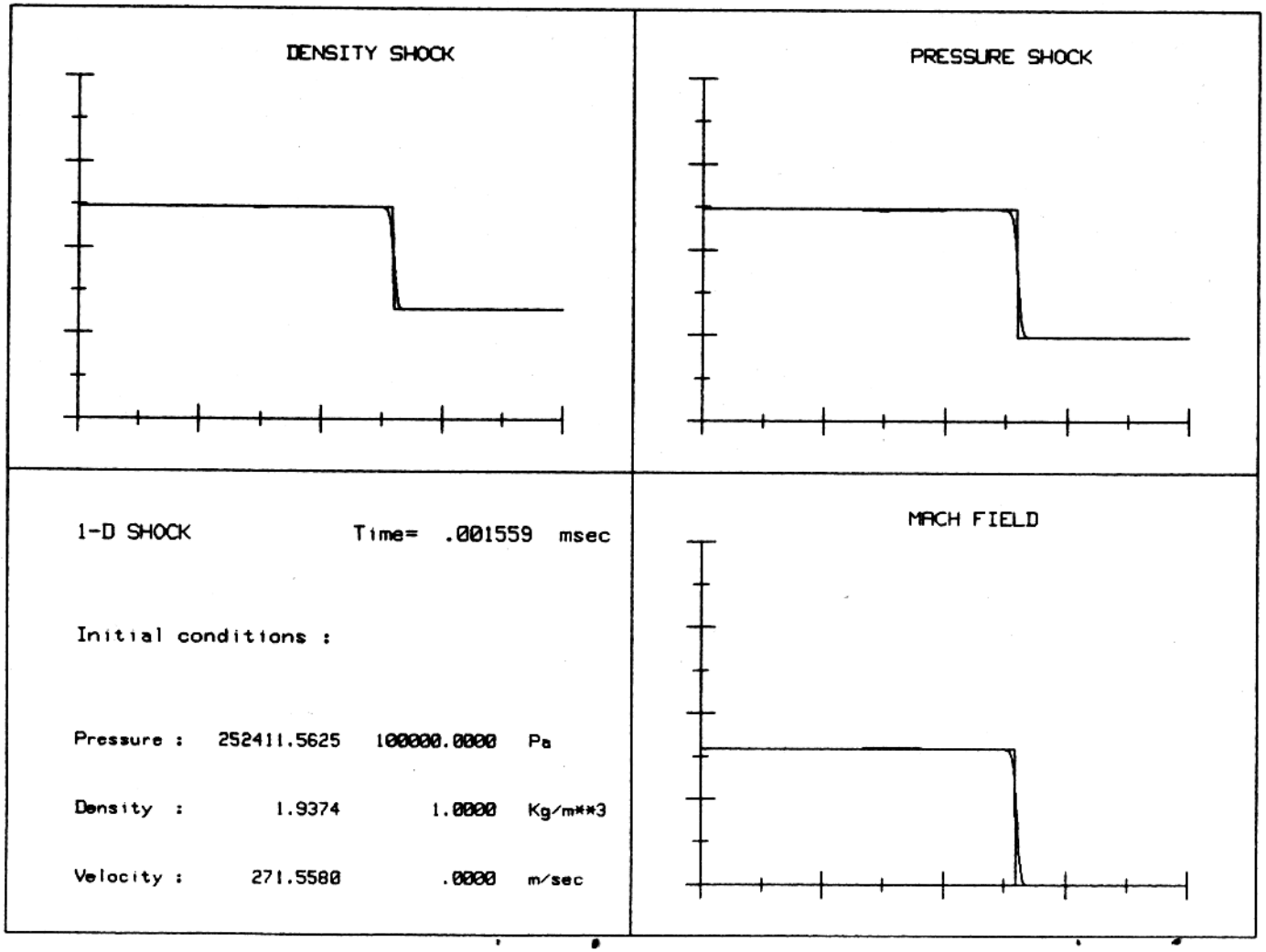

Fig.4.12 1D Shock-Moving Shock Problem

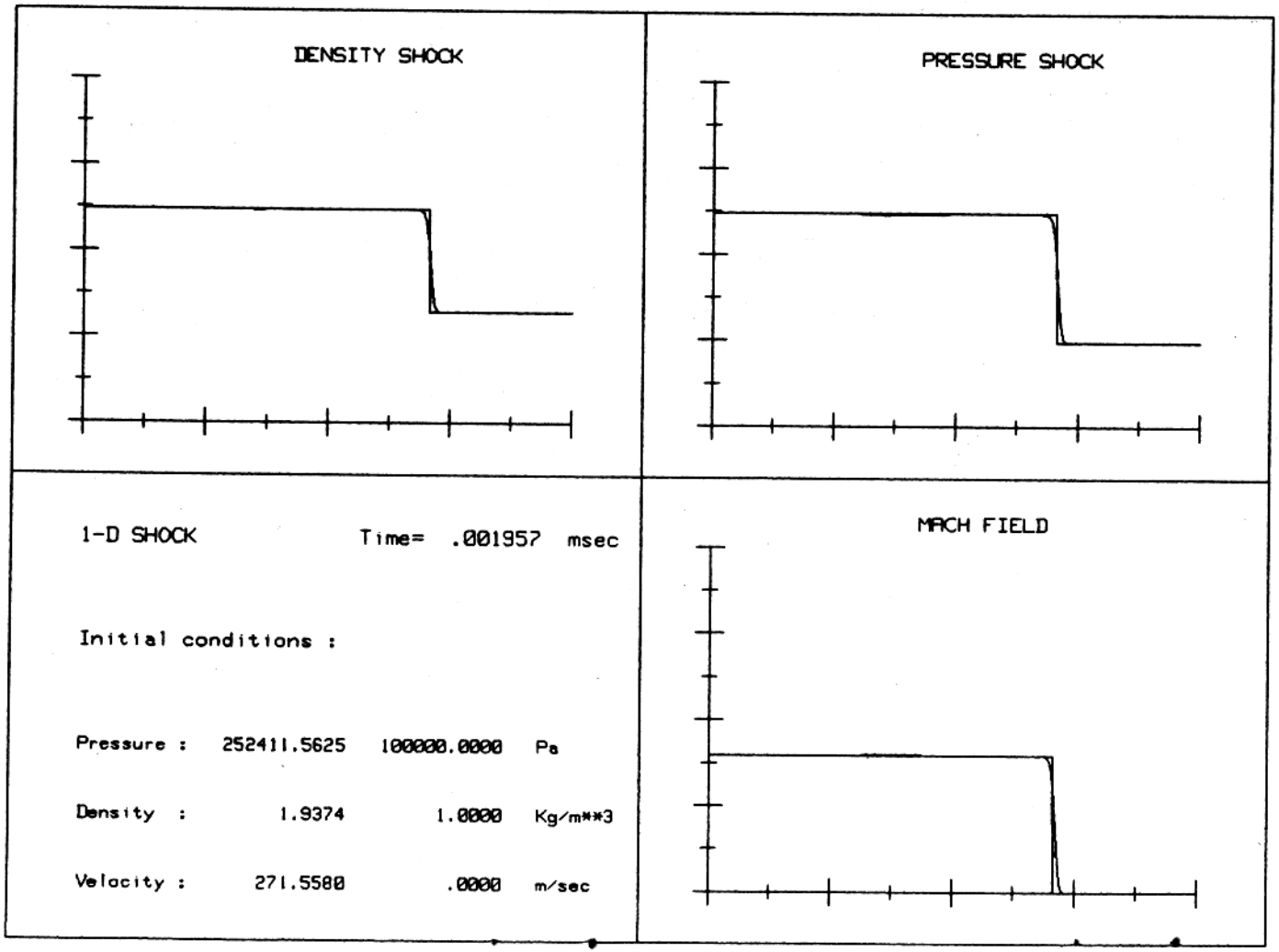

(b) 2D Shock

The problem under consideration here is the flow in a channel passing an obstacle as shown in figure 4.13.

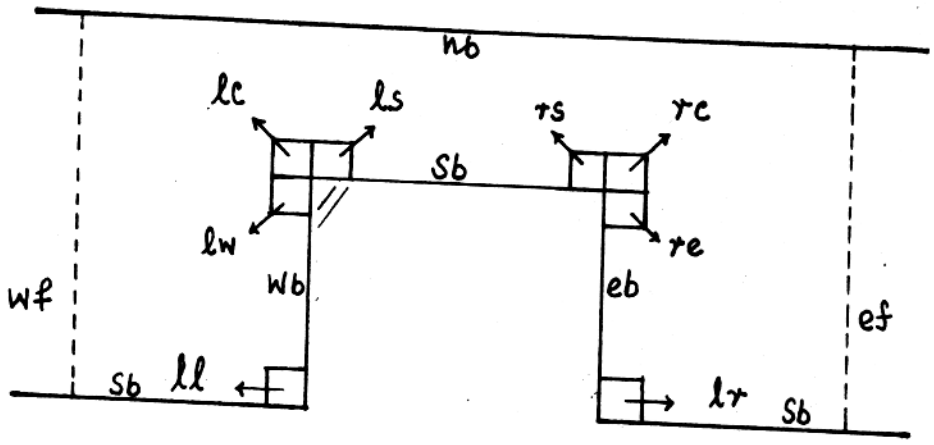

Fig.4.13 2D Flow Past an Obstacle

where ef-east flow; wf-west flow; nb-north boundary; sb-south boundary; eb-east boundary; wb-west boundary; lr-lower right; ll-lower left; lc-left corner; rc-right corner; ls-left south; rs-right south; lw-left west; re-right east.

The cells are taken in such a way that the cells boundaries coincide with the boundary of the channel (Refer fig.4.13). On the boundary, we have taken specular reflection which causes the change in the flux balance term (eqn.(3.1)), mainly for the boundary cells. Figure 4.14 shows how we are

approximating the corner flux on the boundary cells.

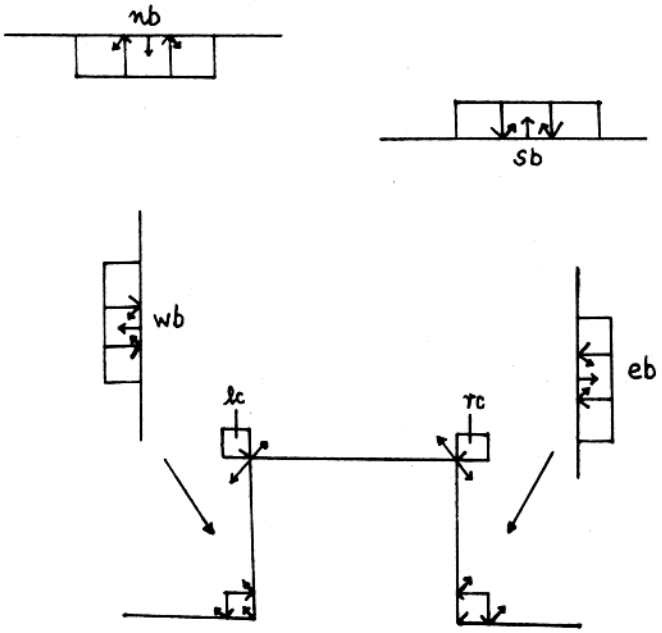

Fig.4.14 Flux Consideration along Boundary

In the above figure, for the cells 'rc' and 'lc', on the corner edge of the boundary, we have taken 50% contribution to each of the other sides. But further investigation is required to check properly how far our criteria on the boundary cells is TRUE. It is still a Question Mark.

The simulation program is written in FORTRAN 77, implemented and tested on HP work station at the University of Kaiserslautern, Germany. The graphical simulations are carried through "STARBASE".

The initial conditions are that of the shock on the left of the obstacle and is given as follows:

p_o=1; ρ_o=1.205; mach=1.12; grid=140×70 {(70-99)×(1-30) for the obstacle}.

The results are exhibited in figures (4.15)-(4.23) for different time levels.

Fig.4.15 Flow Past an Obstacle (2D) (Left of the Obstacle)

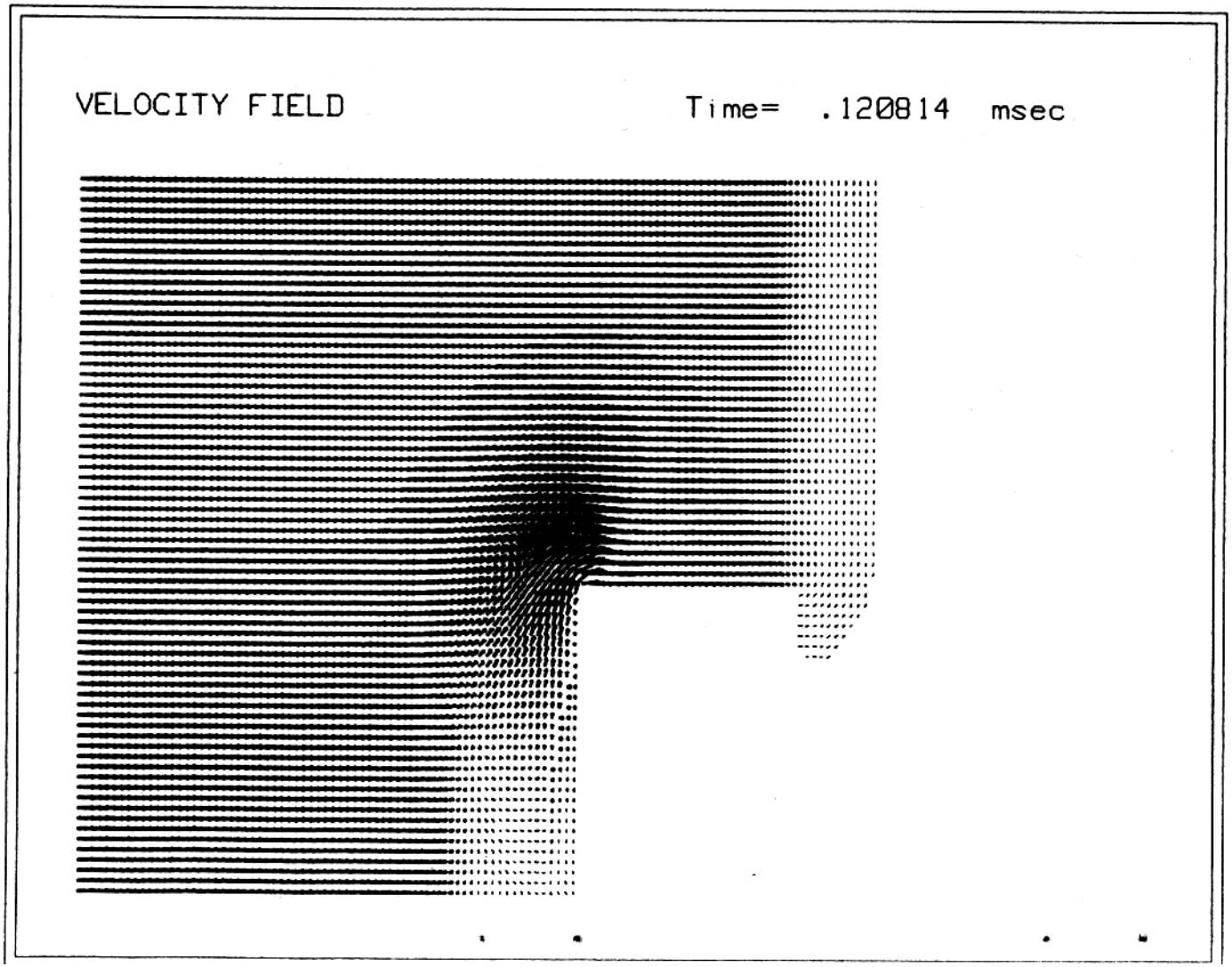

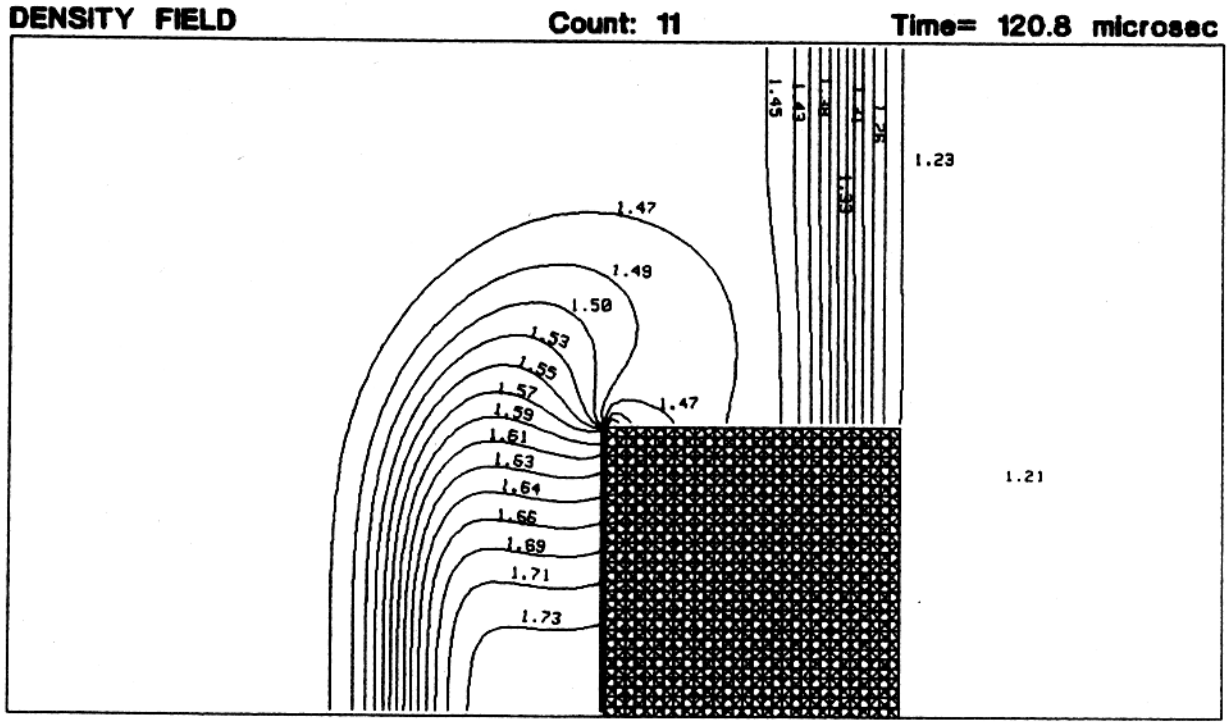

Fig.4.16 Flow Past an Obstacle (2D)

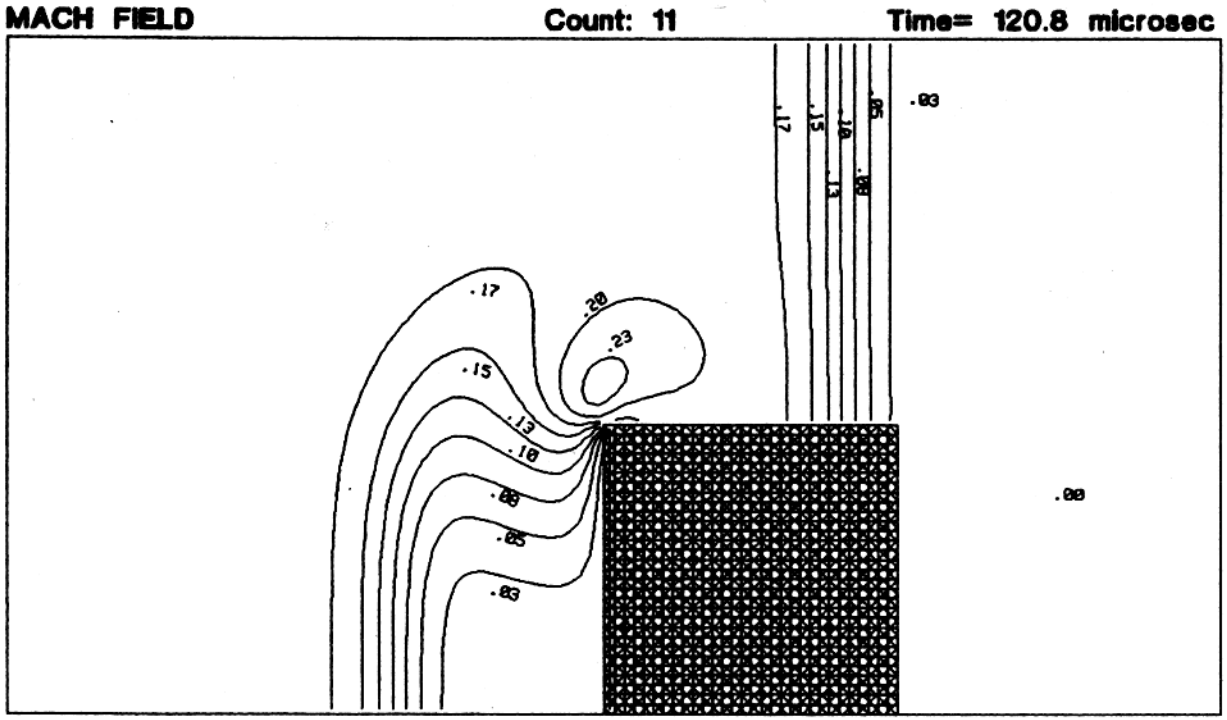

Fig.4.17 Flow Past an Obstacle (2D)

Fig.4.18 Flow Past an Obstacle (2D) (Right of the Obstacle)

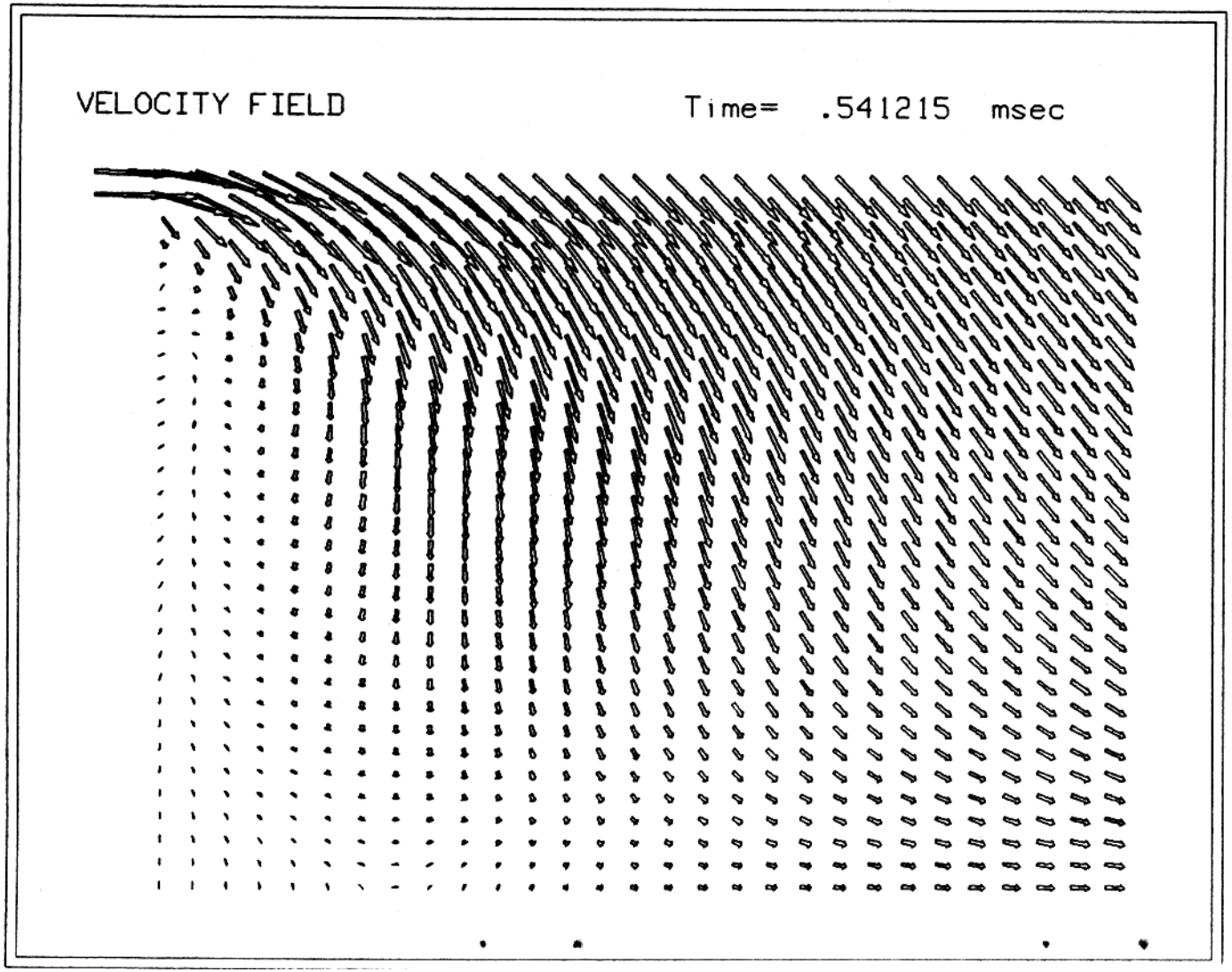

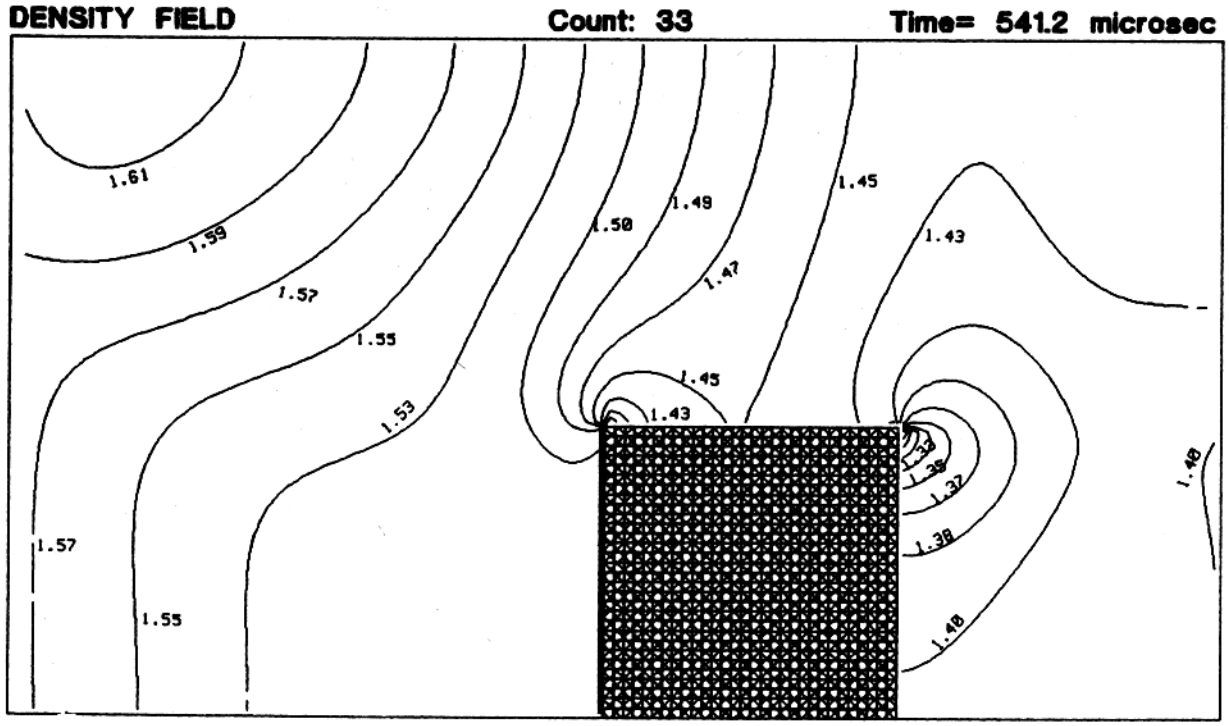

Fig.4.19 Flow Past an Obstacle (2D)

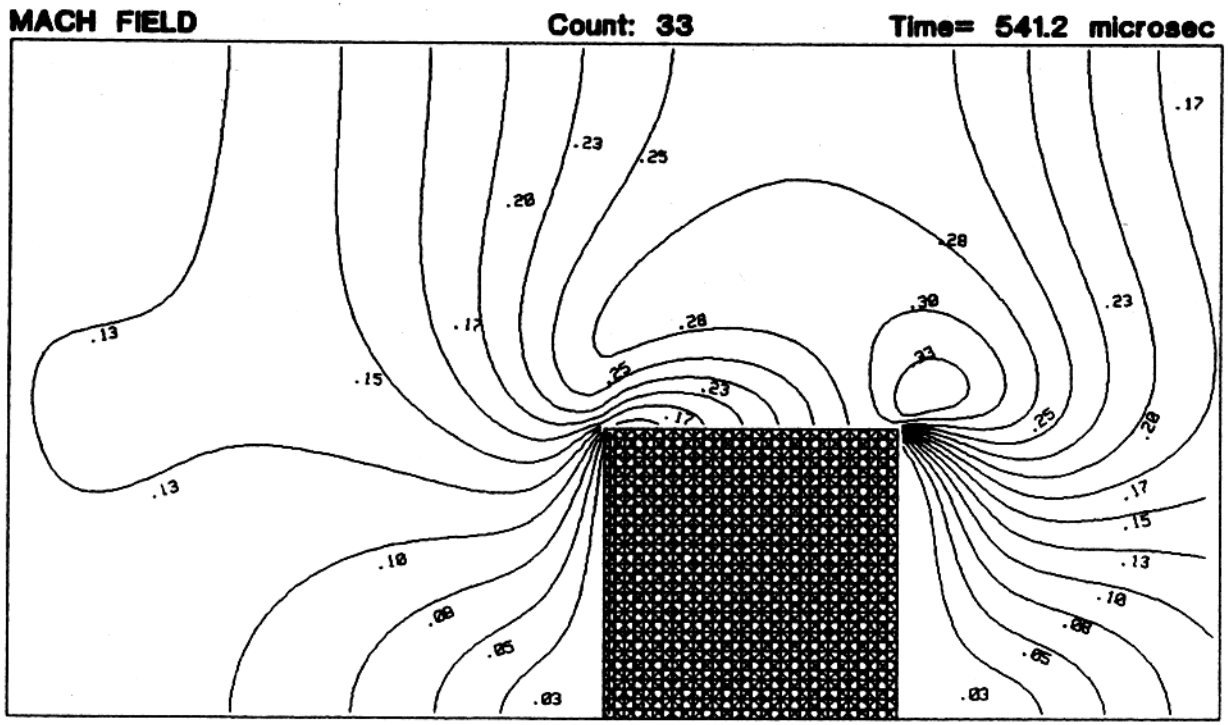

Fig.4.20 Flow Past an Obstacle (2D)

Fig.4.21 Flow Past an Obstacle (2D) (Along the Obstacle)

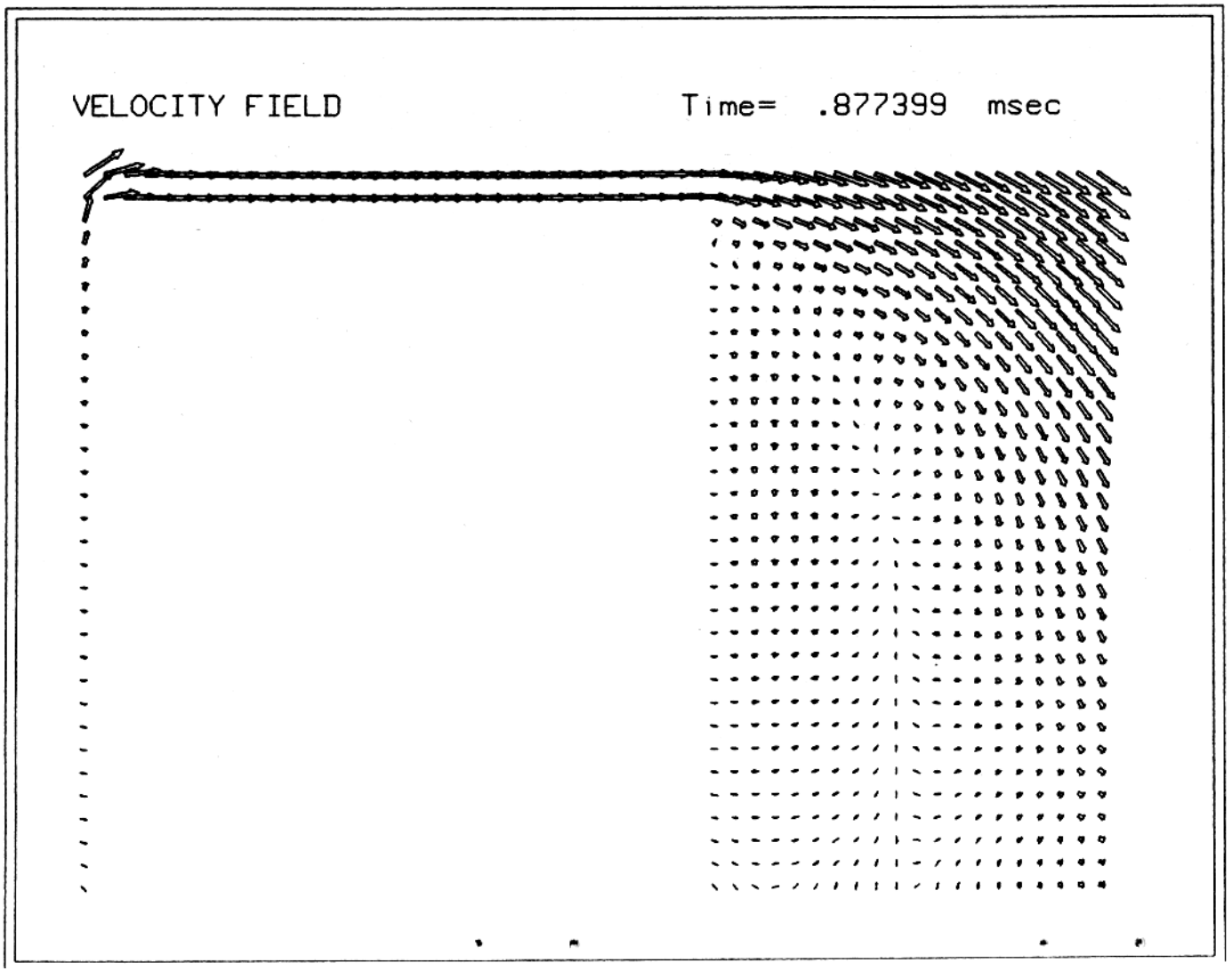

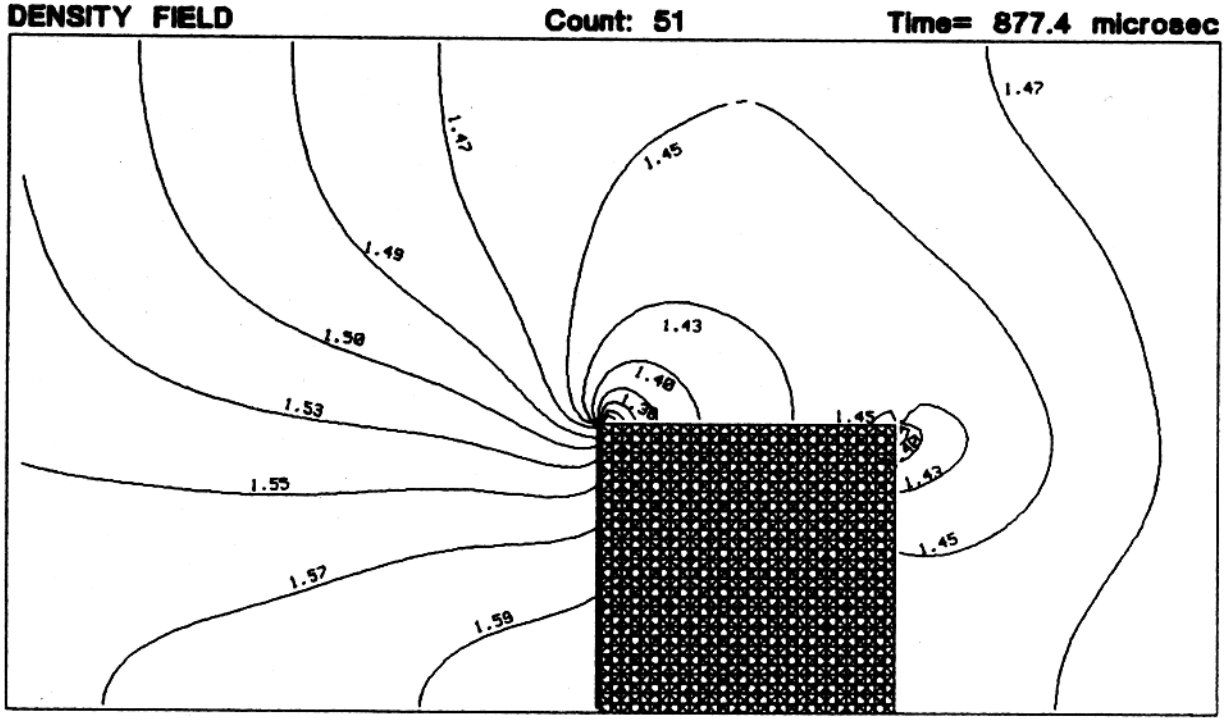

Fig.4.22 Flow Past an Obstacle (2D)

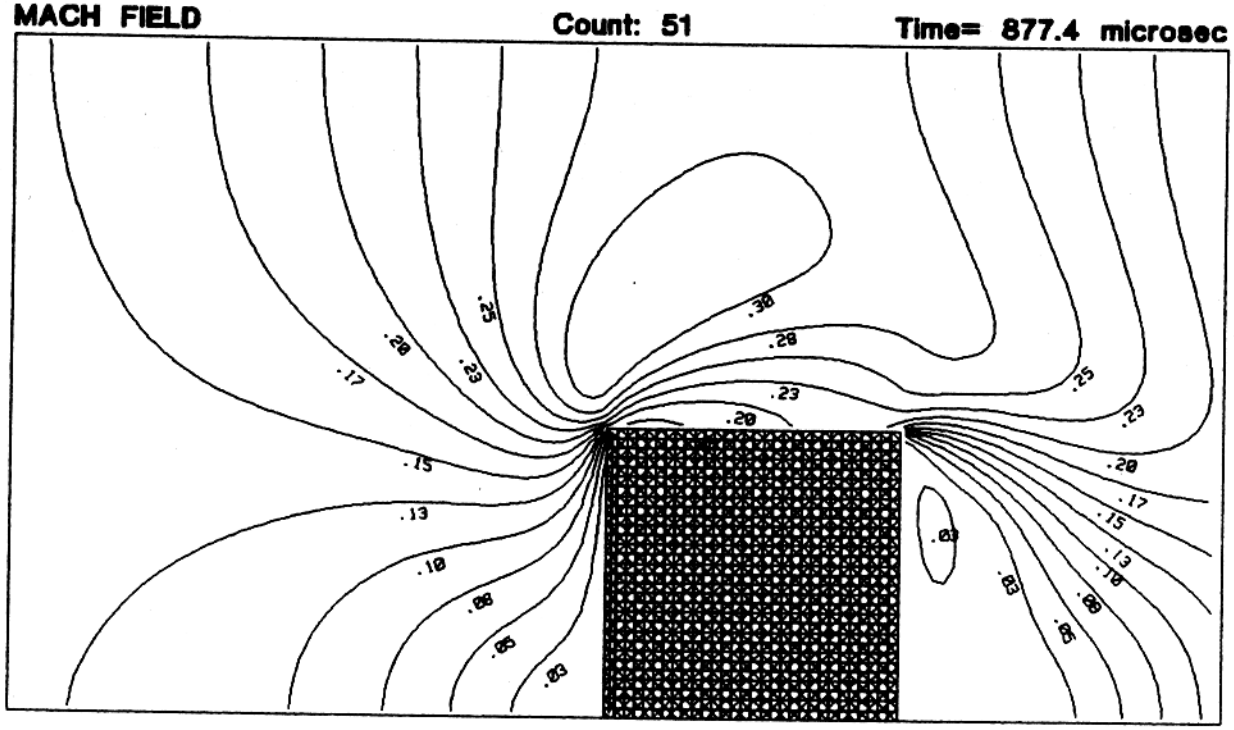

Fig.4.23 Flow Past an Obstacle (2D)

5. Conclusions

With the presentation of the one-step Kaniel kinetical scheme for an isentropic compressible ideal gas (Air), we are making the following final remarks.

The analytic calculations which we have carried out in section 2 is very lengthy. Also the organization of the flux terms is not so easy to handle and one can attempt to make errors in these two steps, which needs careful attention. Though the approach reveals the practical consideration and also it is novel, by experience of dealing the 2D case, we can certainly pin point that the generalization to higher dimensions will be a complicated one.

On the other hand, in the two-step method of Younis[7], one can deal with simple and straight forward logic which makes the algorithm handy. But still further research is required in order to investigate different aspects of the two-step approach mathematically.

The following problems are left under consideration and will be presented in due course:

(1) Our one-step method for the complicated configuration of the flow, i.e. by taking irregular cells, and allowing ρ,u,c to be linear in each cell.

(2) Extensive comparison between one-step and two-step methods and with experimental results.

REFERENCES

[1] S.M. Deshpande and J.C. Mandal, "Kinetic flux-vector splitting (KFVS) for the Euler equation", Report 87 FM 2, Dept. Aerospace Engg., I.I.Sc., Bangalore, 1987.

[2] B. Perthame, "Second order Boltzmann schemes for compressible Euler equations", Rapport de Recherche, No.89-6, Département de Mathématiques, Université d'Orléans, Orléans, 1989.

[3] S. Kaniel, "Approximation of the hydrodynamic equations by a transport process", in: Approximation Methods for Navier-Stokes Problems, Lecture Notes in Mathematics, No.771, 272-286, Springer-Verlag, 1980.

[4] S. Kaniel, "A kinetic model for the compressible flow equations", Indiana Univ. Mathematics J., 37, 537-563, 1988.

[5] S. Kaniel and J. Falcovitz, "Transport approach for compressible flow", 4ème Colloque International sur les Methodes de calcul Scientifique et Technique, North-Holland, 1981.

[6] J.C. Maxwell, The Kinetic Theory of Gases, Collected Works, Dover, 1985.

[7] Suhail Younis, "A two-step kinetical scheme for the solution of the isentropic Euler equations", in preparation.

BISHER SIND FOLGENDE BERICHTE ERSCHIENEN:

Nr. 1 **FORSCHUNG**

W.G. Eschmann und Ralph Götz
Optimierung von Gelenksechsecken

Nr. 2 **WEITERBILDUNG**

H. Neunzert, M. Schulz-Reese
Mathematische Weiterbildung

Nr. 3 **FORSCHUNG**

W. Krüger
The Trippstadt Problem

Nr. 4 **WEITERBILDUNG**

H. Neunzert, M. Schulz-Reese, K.E. Hoffmann
Mathematics in the University and Mathematics in Industry - Complement or Contrast?

Nr. 5 **FORSCHUNG**

A.K. Louis
The Limited Angle Problem in Computerized Tomography

Nr. 6 **FORSCHUNG**

W. Krüger
Regression für Ellipsen in achsenparalleler Lage

Nr. 7 **FORSCHUNG**

Th. Mietzner
Umströmung von Ecken und Kanten, Teil 1

Nr. 8 **FORSCHUNG**

W. Krüger, J. Petersen
Simulation und Extrapolation von Rainflow-Matrizen

Nr. 9 **FORSCHUNG**

W. Krüger, M. Scheutzow u. A. Beste, J. Petersen
Markov- und Rainflow-Rekonstruktionen stochastischer Beanspruchungszeitfunktionen

Nr. 10 **FORSCHUNG**

Th. Mietzner
Umströmung von Ecken und Kanten, Teil 2

Nr. 11 **FORSCHUNG**

H. Ploss
Simulationsmethoden zur Lösung der Boltzmanngleichung

Nr. 12 **FORSCHUNG**

M. Keul
Mathematische Modelle für das Zeitverhalten stochastischer Beanspruchungszeitfunktionen

Nr. 13 **AUSBILDUNG**

W. Krüger, H. Neunzert, M. Schulz-Reese
Fundamentals of Identification of Time Series

Nr. 14 **FORSCHUNG**

H. Moock
Ein mathematisches Verfahren zur Optimierung von Nocken

Nr. 15 **FORSCHUNG**

F.-J. Pfreundt
Berechnung und Optimierung des Energiegewinnes bei Anlagen zur Lufterwärmung mittels Erdkanal

Nr. 16 **FORSCHUNG**

F.-J. Pfreundt
Berechnung einer 2-dimensionalen Kanalströmung mit parallel eingeblasener Luft

Nr. 17 **FORSCHUNG**

G. Alessandrini
Some remarks on a problem of sound measurements from incomplete data

Nr. 18 **AUSBILDUNG**

W. Diedrich
Einfluß eines Latentwärmespeichers auf den Wärmefluß durch eine Ziegelwand

Nr. 19 **FORSCHUNG**

M. Stöhr
Der Kalman-Filter und seine Fehlerprozesse unter besonderer Berücksichtigung der Auswirkung von Modellfehlern

Nr. 20 **FORSCHUNG**

H. Babovsky
Berechnung des Schalldrucks im Innern eines Quaders

Nr. 21 **FORSCHUNG**

W.G. Eschmann
Toleranzuntersuchungen für Druckmessgeräte

Nr. 22 **FORSCHUNG**

G. Schneider
Stratification of solids, a new perspective in three dimensional computer aided design

Nr. 23 **FORSCHUNG**

H.-G. Stark
Identifikation von Amplituden und Phasensprüngen im Intensitätsverlauf eines Nd-YAG Festkörperlasers

Nr. 24 **FORSCHUNG**

M. Scheutzow
Einfache Verfahren zur Planung und Auswertung von Navigationsversuchsfahrten

Nr. 25 **FORSCHUNG**

G.R. Dargahi-Noubary
A Parametric Solution for Simple Stress-Strength Model of Failure with an Application

Nr. 26 **FORSCHUNG**

U. Helmke, D. Prätzel-Wolters
Stability and Robustness Properties of Universal Adaptive Controllers for First Order Linear Systems

Nr. 27 **FORSCHUNG**

G. Christmann
Zeitreihen und Modalanalyse

Nr. 28 **FORSCHUNG**

H. Neunzert, B. Wetton
Pattern recognition using measure space metrics

Nr. 29 **FORSCHUNG**

G. Steinebach
Semi-implizite Einschrittverfahren zur numerischen Lösung differential-algebraischer Gleichungen technischer Modelle

Nr. 30 **FORSCHUNG**

Martin Brokate
Properties of the Preisach Model for Hysteresis

Nr. 31 **FORSCHUNG**

H.-G. Stark, H. Trinkaus, Ch. Jansson
The Simulation of the Charge Cycle in a Cylinder of a Combustion Engine

Nr. 32 **FORSCHUNG**

H. Babovsky, F. Gropengießer, H. Neunzert
J. Struckmeier, B. Wiesen
Low Discrepancy Methods for the Boltzmann Equation

Nr. 33 **FORSCHUNG**

M. Brokate
Some BV properties of the Preisach hysteresis operator

Nr. 34 **FORSCHUNG**

H. Neunzert
Industrial Mathematics: General Remarks and Some Case Studies

Nr. 35 **FORSCHUNG**

M. Brokate
On a Characterization of the Preisach Model for Hysteresis

Nr. 36 **FORSCHUNG**

C.-P. Fritzen, P. Hackh
Optimization of a Spring for Dental Attachments

Nr. 37 **FORSCHUNG**

U. Helmke, D. Prätzel-Wolters, S. Schmid
Adaptive Synchronization of Interconnected Linear Systems

Nr. 38 **FORSCHUNG**

U. Helmke, D. Prätzel-Wolters, S. Schmid
Sufficient Conditions for Adaptive Stabilization and Tracking

Nr. 39 **FORSCHUNG**

U. Helmke, D. Prätzel-Wolters, S. Schmid
Adaptive Tracking for Scalar Minimum Phase Systems

Nr. 40 **FORSCHUNG**

F.-J. Pfreundt
Nähen als dynamisches System

Nr. 41 **FORSCHUNG**

H.-G. Stark
Multiscale Analysis, Wavelets and Texture Quality

Nr. 42 **FORSCHUNG**

I. Einhorn, H. Moock
A Deterministic Particle Method for the Simulation of the Boltzmann Transport Equation of Semiconductors

Nr. 43 **FORSCHUNG**

F. Gropengießer, H. Neunzert, J. Struckmeier
Computational Methods for the Boltzmann Equation

Nr. 44 **FORSCHUNG**

S. Nikitin, S. Schmid
Universal Adaptive Stabilizers for One-Dimensional Nonlinear Systems

Nr. 45 **FORSCHUNG**

P. Hackh
Quality Control of Artificial Fabrics

Nr. 46 **FORSCHUNG**

S. Körber, B. Wiesen
A Comparison of a Microscopic and a Phenomenological Model for a Polyatomic Gas

Nr. 47 **FORSCHUNG**

F. Gropengießer, H. Neunzert,
J. Struckmeier, B. Wiesen
Several Computer Studies on Boltzmann Flows in Connection with Space Flight Problems

Nr. 48 **FORSCHUNG**

M. Brokate
Some Remarks on the Discretization of the Preisach Operator

Nr. 49 **FORSCHUNG**

M. Brokate
On the Mowing Preisach Model

Nr. 50 **FORSCHUNG**

W. Wagner
A Stochastic Particle System Associated with the Spatially Inhomogeneous Boltzmann Equation

Nr. 51 **AUSBILDUNG** (interner Bericht)

I.M. Sobol
Punkte, die einen mehrdimensionalen Würfel gleichmäßig ausfüllen

Nr. 52 **FORSCHUNG**

M. Brokate, A.H. Siddiqi
Sensitivity in the Rigid Punch Problem

Nr. 53 **FORSCHUNG**

S. Nikitin, D. Prätzel-Wolters
Multiparameter, Polynomial Adaptive Stabilizers

Nr. 54 **FORSCHUNG**

S. Schmid, D. Prätzel-Wolters
Synchronization through System Interconnections

Nr. 55 **FORSCHUNG**

D. Prätzel-Wolters, R.D. Reinke
Simple Adaptive Control of a Discrete Almost Strict Positive Real Heat Treatment System

Nr. 56 **FORSCHUNG**

S. Chen, D. Prätzel-Wolters
Modelling and Controller Design for Heat Treatment Processing of Enamelled Wires

Nr. 57 **FORSCHUNG**

B. Wiesen
On the Dependence of the Solution of Generalized Boltzmann Equations on the Scattering Cross Section: The Inverse Problem

Nr. 58 **FORSCHUNG**

G. Engl, R. Rösch
Studien zum Programmsystem PROMO (Berechnung des instationären Ladungswechsels von zündenden Mehrzylinder-Verbrennungsmotoren)

Nr. 59 **FORSCHUNG**

J. Hoffmann, D. Prätzel-Wolters
Controllability Tests for Behaviour Systems in AR-Representations

Die Berichte der Arbeitsgruppe Technomathematik können angefordert werden bei:

UNIVERSITÄT KAISERSLAUTERN
Fachbereich Mathematik
Arbeitsgruppe Technomathematik
Postfach 3049

6750 Kaiserslautern